# Chapter 4

# Interaction with Cavity Standing Waves

As mentioned in Chapter 1, the electromagnetic fields form simple standing wave patterns within a cylindrical cavity, which are ideal for radiative studies. Splitting the metallic walls of a cylindrical cavity to form the electrodes of a Penning trap allows electrons to be confined in a region smaller than the characteristic wavelength of a cavity standing wave. Radiative cooling of localized electrons in a resonant cavity mode, in fact, is crucial for demonstrating many of the collective behaviors in parametrically-pumped electron oscillators, presented in Chapter 3. The extreme sensitivity of synchronized motions to radiative cooling provides a new technique for probing the standing wave modes of a Penning trap cavity, *in situ* at 4 K without any microwave drive. We now discuss the interesting effects which are observed, and important applications which are possible, when electrons interact with well-characterized radiation fields.

## 4.1 Observing Microwave Cavity Modes Below 166 GHz

Despite great attention to making a cylindrical Penning trap cavity which is a good approximation to an ideal cylindrical cavity, the small slits, holes and uncontrolled imperfections unavoidably shift the radiation eigenfrequencies of the

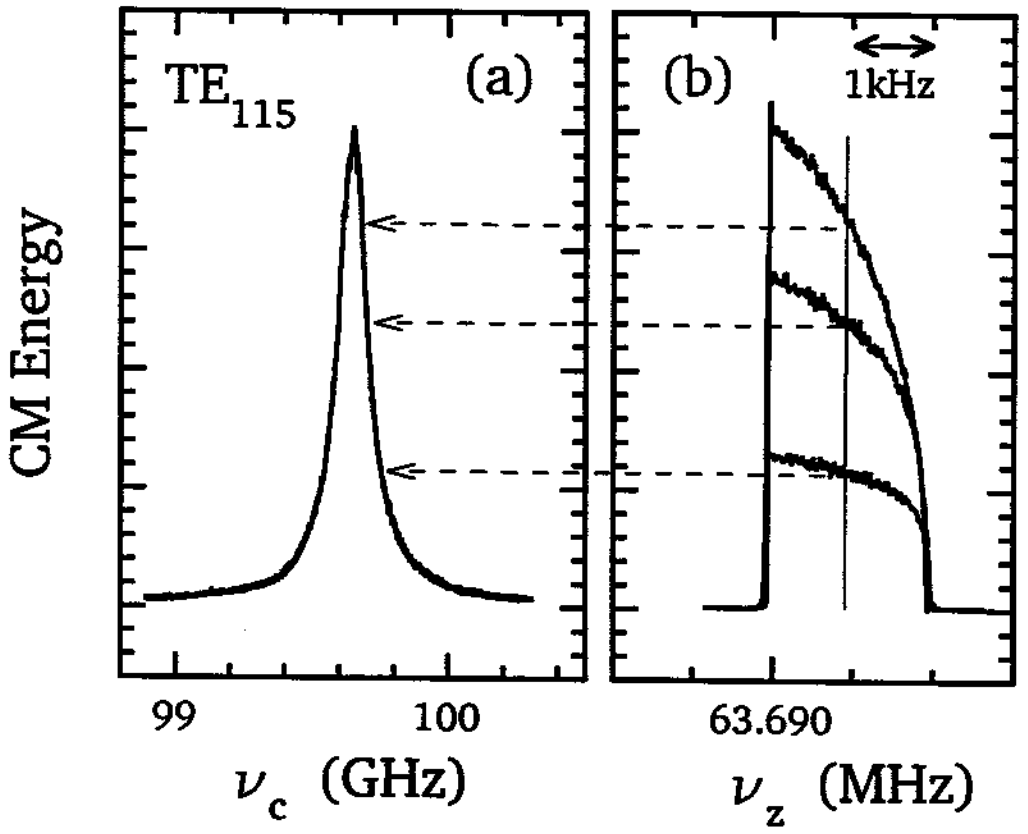


Figure 4.1: (a) Cavity resonance observed by monitoring the axial CM energy while slowly sweeping the magnetic field to vary $\omega_c'$, with pump frequency at $\omega_d = 2\omega_z$ and pump strength $h = 1.3h_T$. (b) Parametric axial resonances for indicated cyclotron frequencies.

trap cavity from those of an ideal cylindrical cavity. The hope is that the shifts are small, so that measured eigenfrequencies can still be used to identify the modes. Furthermore, small shifts would indicate that the standing wave fields in the trap cavity are essentially the simple analytic forms discussed above.

A simplified diagram of the system with detection electronics is depicted in Fig. 2.17. To insure that parametric resonance is sustained during mode detection, the parametric pump is prepared in the region of (Mathieu's) instability in $(h, \omega_d)$ space, in which the quiescent state is unstable. This region is cross-hatched in

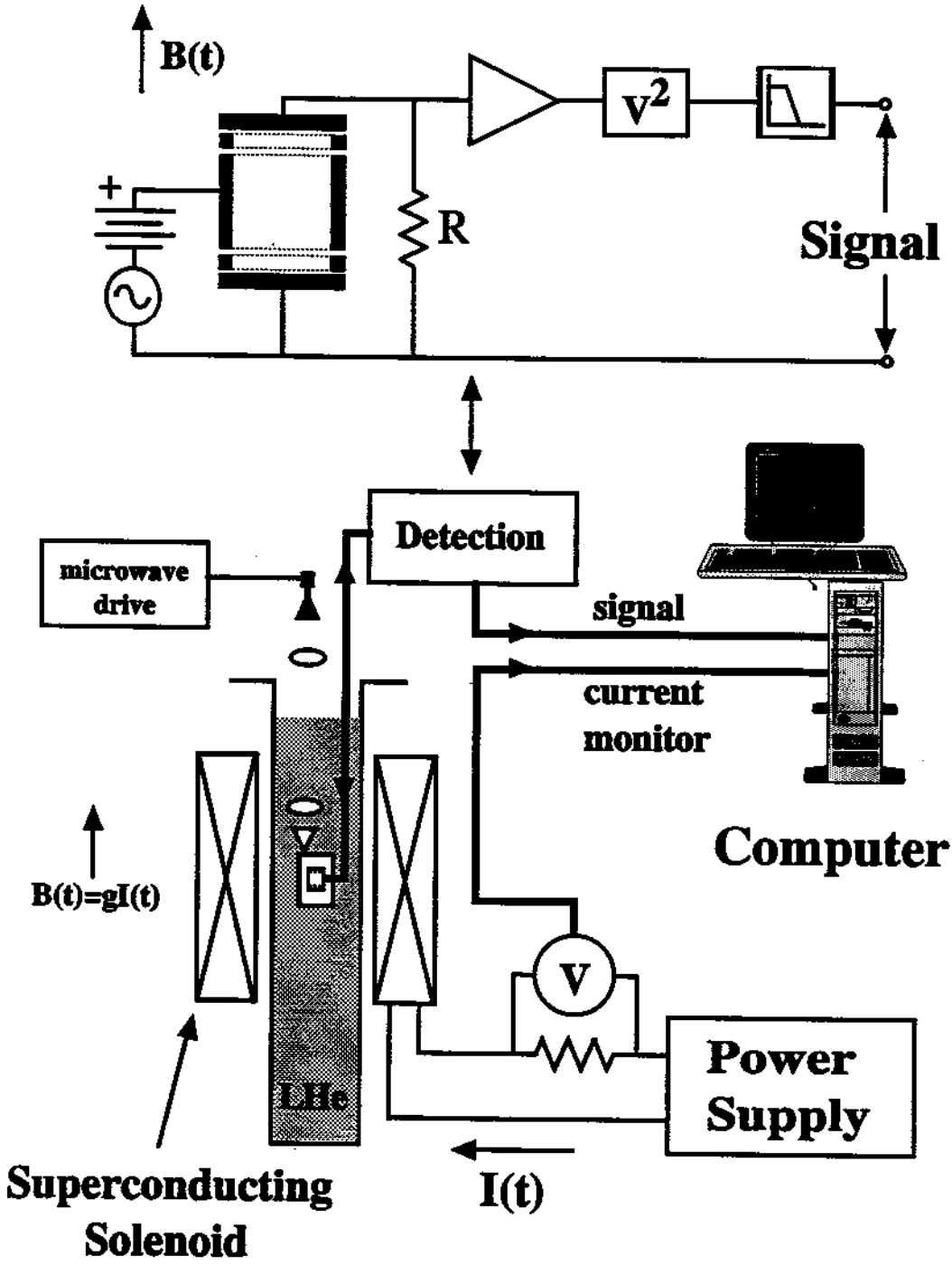


Figure 4.2: Simplified diagram of the experimental apparatus for cavity mode detection.

Fig. 3.3. Fig. 4.1b shows the measured frequency response with the pump strength held fixed at a value above the threshold. This family of superimposed resonances is obtained by varying the detuning between the cavity mode frequency and the electron cyclotron frequency. It clearly shows that the signal grows with increasing radiative cooling and reaches a maximum when the cyclotron frequency is swept into resonance with the cavity mode. Cavity modes are thus conveniently detected by fixing the pump frequency at $\omega_d = 2\omega_z$ and monitoring the axial CM energy, while the cyclotron frequency is being swept, as illustrated in Fig. 4.1a. A simplified overview of the full apparatus is shown in Fig. 4.2. The trap is sealed in a high-vacuum envelope, which is cryopumped via thermal contact with a liquid helium bath. The magnetic field is generated by a superconducting solenoid designed for precise studies with nuclear magnetic resonance. Since the cyclotron frequency is proportional to the magnetic field, we sweep the current in the superconducting solenoid up to 5.9 Tesla (slowly, because the solenoid inductance is 200 Henries) in order to tune the cyclotron oscillators into resonance with one cavity mode after another. A measure of the current in the solenoid and the signal from the electron oscillators are digitized simultaneously and stored in a computer. (A conversion from measured solenoid current to cyclotron frequency is obtained by exciting an electron cyclotron resonance with a microwave source.) A 50 GHz wide spectrum is shown in Fig. 4.3 (without any microwave drive). The full spectrum of observed cavity modes between 0 to 166 GHz is presented in Fig. 4.14 and takes about 10 hrs to obtain. The extraordinary sensitivity of the synchronized motion of the electron oscillators to radiative cooling via energy transfer to the modes of the trap cavity allows us to observe even weakly coupled cavity modes (e.g., those with nodes in the midplane), presumably because the electrons occupy a volume extending slightly away from the center of the trap. Isolated resonances have Lorentzian lineshapes, as illustrated by the data points and Lorentzian fits for the two modes in Fig. 4.4. Thermal cycling of the trap apparatus up to 300 K and back to 4.2 K changes the observed resonance frequencies by less than 0.1%.

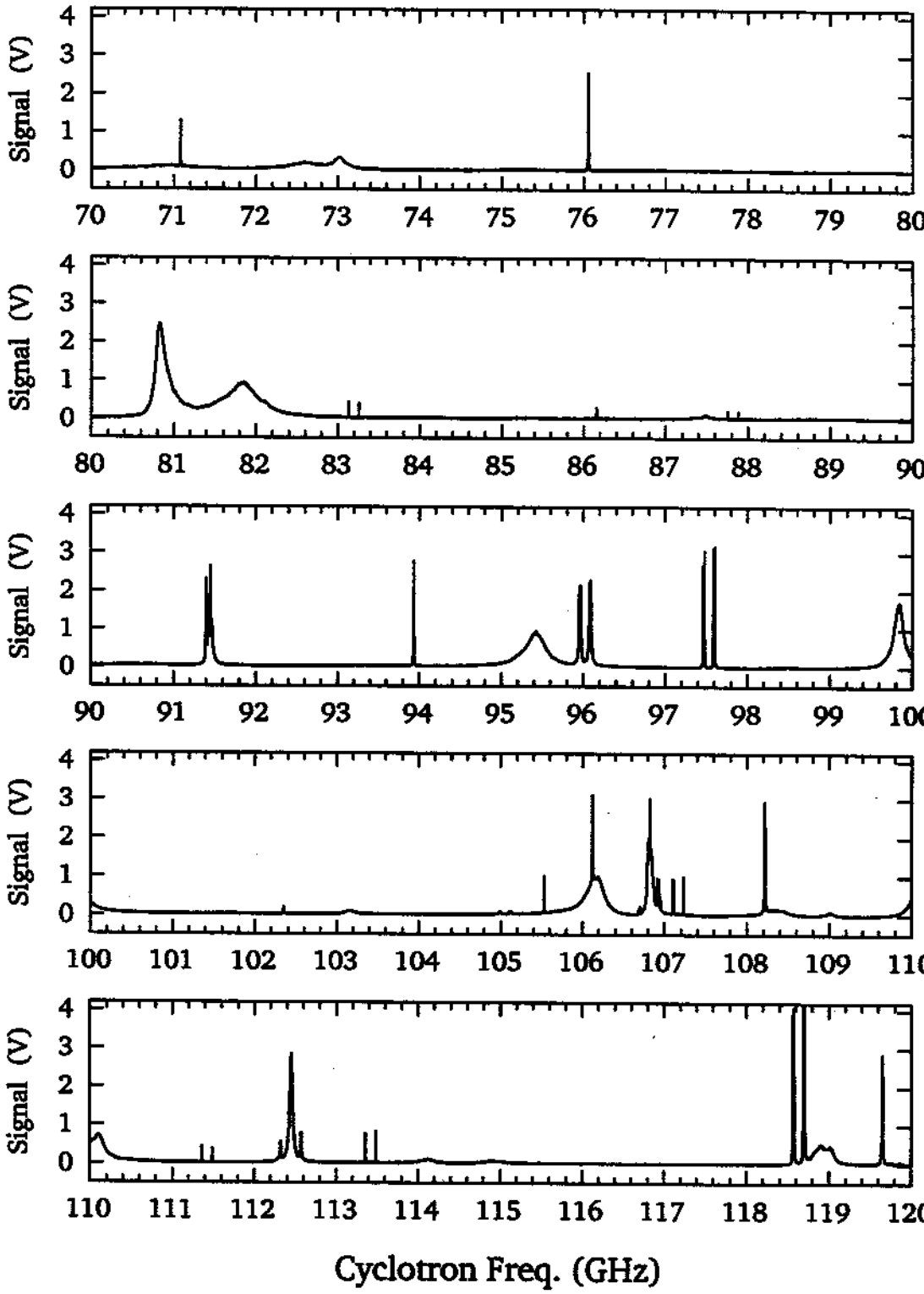


Figure 4.3: Observed cavity modes between 70 and 120 GHz.

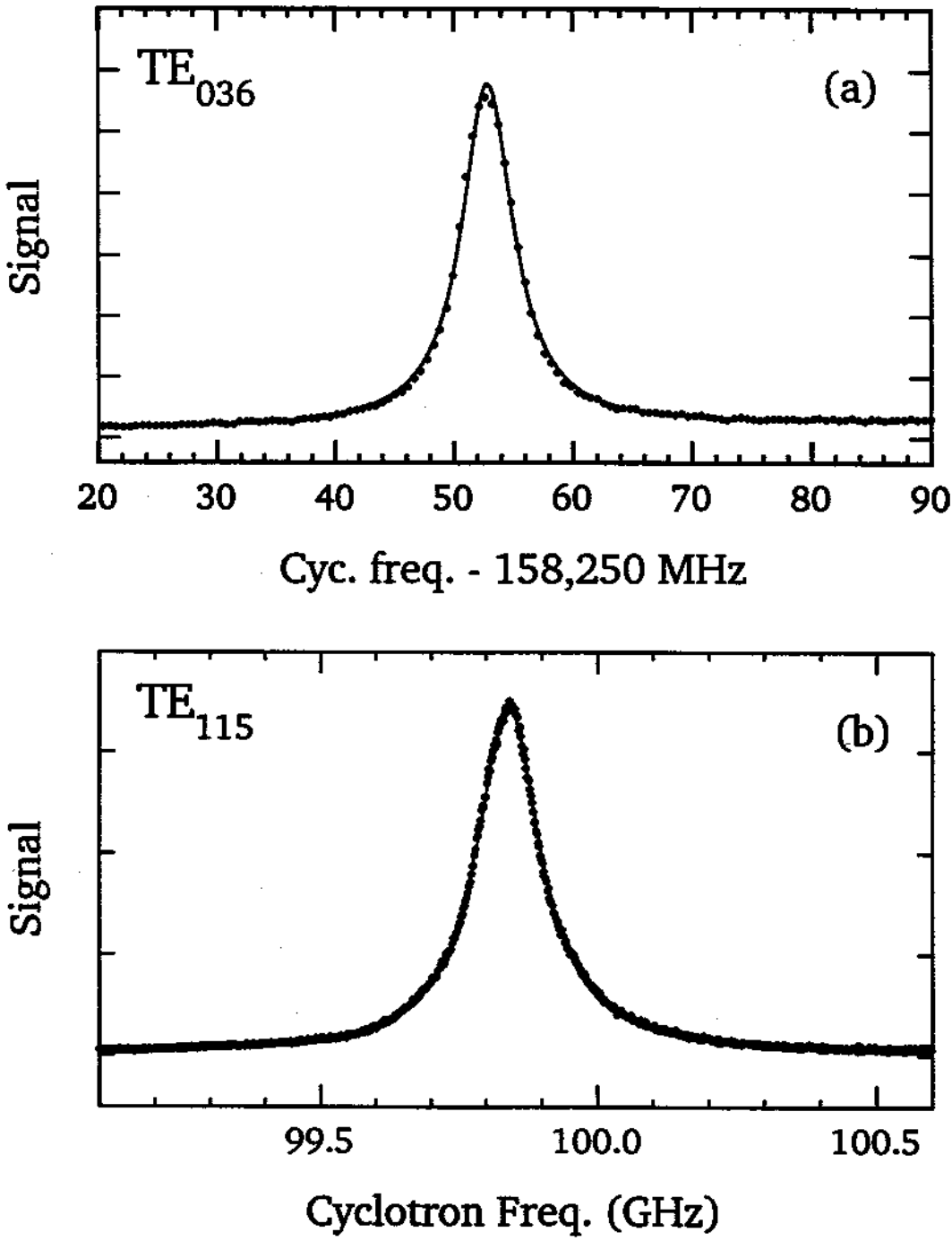


Figure 4.4: Lorentzian lineshapes (solid lines) fit to observed cavity modes (dots) which are well separated from other modes.

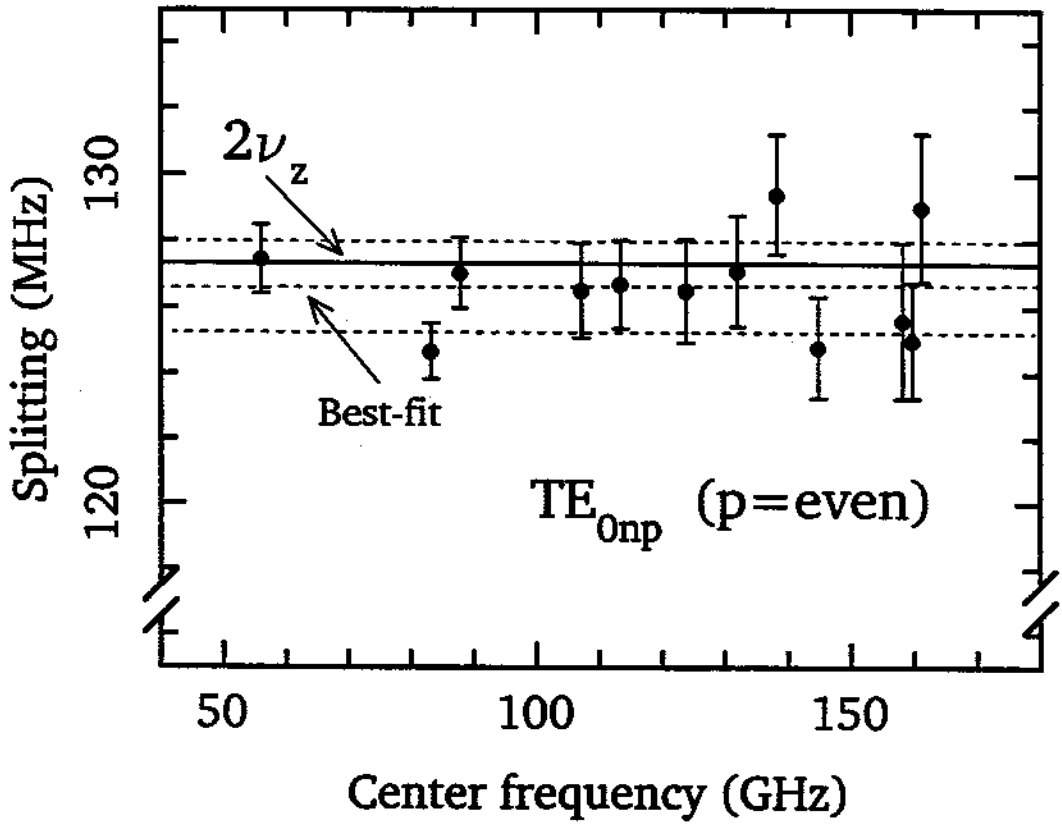


Figure 4.5: Motional splitting of singlet modes $TE_{0np}$. The best fit (center dashed line) is consistent with $2\nu_z$ (solid line) within its uncertainty (dashed lines above and below).

### 4.1.1 Motional Effects

The $TE_{0np}$ modes are unusual in that these azimuthally symmetric modes are singlets, unlike $m > 0$ modes which are doubly degenerate. In the observed spectrum, however, $TE_{0np}$ resonances with even $p$ appear near the frequencies expected for an ideal cylinder in Eq. (2.1), but they appear as doublets. Modes with $p$ even have a node in the midplane of the trap and are thus decoupled from the cyclotron motion of electrons located exactly at the center of the trap. The periodic axial motion of the electrons, driven by the parametric pump, makes the electrons sample the standing wave field away from the node at the center of the trap. The

microwave field experienced by the oscillating electrons is thus amplitude modulated, which produces the observed sidebands. Plotting the frequency separations for the doublets (Fig. 4.5) shows clearly that the splittings are twice the axial oscillation frequency as would be expected. All even p modes, regardless of $m$ value, give similar motional splitting in the spectrum, as illustrated in Fig. 4.6a. The motional effect is different (and typically smaller) for odd $p$ modes since these have a maximum of the standing wave field at the center of the trap. Nevertheless, for sufficiently large oscillations and for large $p$, small sidebands are observed at $2\nu_z$ to either side of the strong central peak as illustrated in Fig. 4.6b.

### 4.1.2 Comparison with Ideal Cavity

With motional sidebands understood, the measured frequencies correspond well to those for a perfect cylindrical cavity, offering the possibility of identifying resonant modes of a trap cavity for the first time. The azimuthally-symmetric TE modes with $m = 0$ have high Q values and are not shifted much by the slits because induced surface currents flow parallel to the slits, allowing the effective trap dimensions to be determined *in situ* at 4 K to within 6 $\mu$m, as shown in Fig. 4.7. A best fit of Eq. (2.1) to 12 measured eigenfrequencies for such modes yields a rms frequency deviation of 0.08% and dimensions $\rho_0 = 0.4559(6)$ cm and $z_0 = 0.3838(6)$ cm, in good agreement with our expectations based upon machining tolerances and expected thermal contraction. Taking the observed width at half maximum divided by the resonant frequency to be $Q^{-1}$, the mean Q is 20,000 with an rms spread of 6500.

For other field symmetries of experimental interest, Fig. 4.8 shows percentage deviations of measured and calculated resonant frequencies. There is good agreement. The most important modes [9,10,37], those with $p$ odd and $m = 1$, have nonvanishing transverse electric fields at the cavity center and hence couple directly to the small cyclotron orbit of an electron. The strong coupling results in the largest observed resonance signals (i.e. largest peak area in Fig. 4.3) for the 29

of these modes which we observe. Frequency deviations are typically 1%, which is larger than for the $TE_{0np}$ modes above as expected. Nonetheless, the shifts are still typically 5 times smaller than the average mode spacing, though mode overlap gets more likely as the mode density increases at higher frequencies. The mean Q is 1300, with a spread of 1100 and a highest Q of 3700.

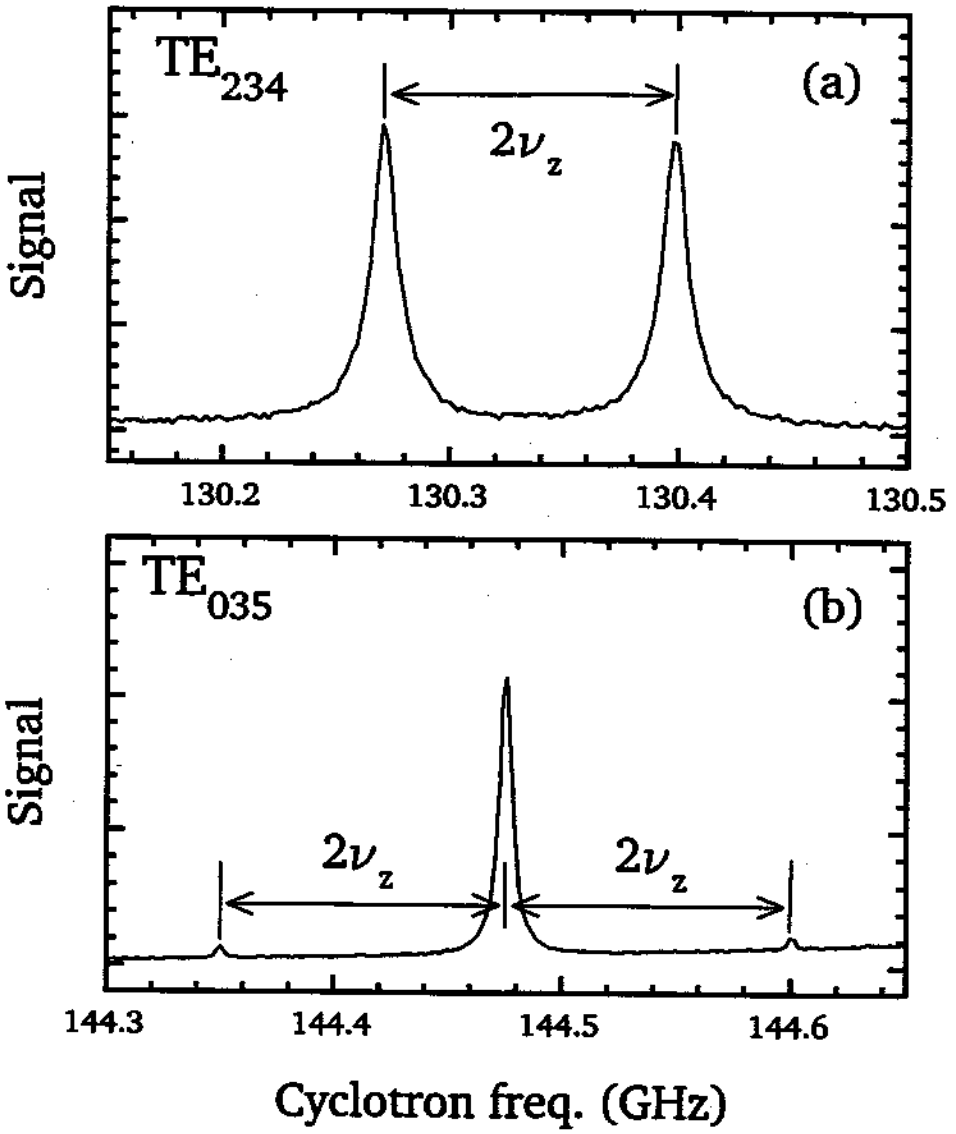


Figure 4.6: (a) Motional doublet for a mode with p even has separation of $2\nu_z$. (b) Motional sidebands for a mode with odd p are separated from the strong central peak by $2\nu_z$.

### 4.1.3 Strong Coupling

Isolated modes fit well to Lorentzian lineshapes, as has been illustrated. Fig. 4.9 illustrates the lineshape modification which occurs when an electron cloud and a cavity mode are strongly coupled. A Lorentzian lineshape (Fig. 4.9a) is observed with small number of electrons. For weak coupling, the decay rate of one electron cyclotron oscillator coupled to the $M$th cavity mode is, as we shall see later, given

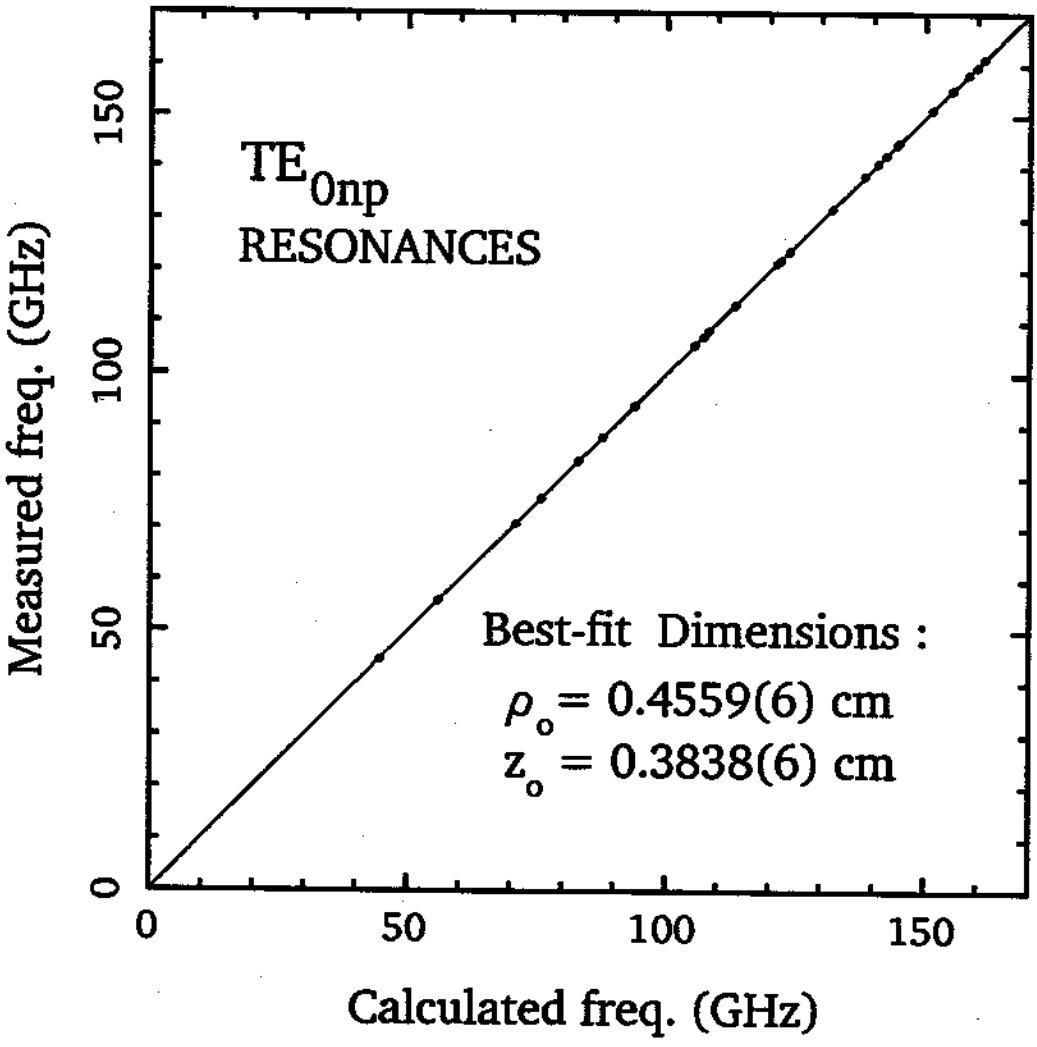


Figure 4.7: Fit of measured $TE_{0np}$ mode eigenfrequencies to those calculated for an ideal cylinder , in situ at 4K, determines effective dimensions of the trap cavity to within 6 $\mu$m.

| Mode | Eigenfrequency (GHz) | $\gamma_M/Q_M\gamma_c$ |
|---|---|---|
| $TE_{111}$ | 27.435 | 0.8295 |
| $TM_{111}$ | 44.608 | 0.0542 |
| $TE_{121}$ | 59.124 | 0.1709 |
| $TE_{113}$ | 61.667 | 0.0732 |
| $TM_{113}$ | 70.993 | 0.0480 |
| $TM_{121}$ | 75.986 | 0.0068 |
| $TE_{123}$ | 80.905 | 0.0668 |
| $TE_{131}$ | 91.461 | 0.0724 |
| $TM_{123}$ | 93.936 | 0.0213 |
| $TE_{115}$ | 99.513 | 0.0174 |
| $TM_{115}$ | 105.547 | 0.0184 |
| $TE_{133}$ | 106.842 | 0.0455 |
| $TM_{131}$ | 108.265 | 0.0017 |
| $TE_{125}$ | 112.454 | 0.0249 |
| $TM_{133}$ | 121.538 | 0.0085 |
| $TM_{125}$ | 122.165 | 0.0159 |
| $TE_{141}$ | 124.077 | 0.0395 |
| $TE_{135}$ | 132.346 | 0.0239 |
| $TE_{143}$ | 135.813 | 0.0302 |
| $TE_{117}$ | 138.033 | 0.0065 |
| $TM_{141}$ | 140.824 | 0.0006 |
| $TM_{117}$ | 142.444 | 0.0080 |
| $TM_{135}$ | 144.470 | 0.0099 |
| $TE_{127}$ | 147.635 | 0.0110 |
| $TM_{143}$ | 151.267 | 0.0037 |
| $TM_{127}$ | 155.159 | 0.0094 |
| $TE_{145}$ | 156.670 | 0.0197 |
| $TE_{151}$ | 156.803 | 0.0248 |
| $TE_{137}$ | 163.296 | 0.0128 |
| $TE_{153}$ | 166.245 | 0.0208 |

Table 4.1: Calculated properties of $m = 1$, $p$ odd modes below 170 GHz for an ideal cavity which has the best-fit dimensions of the trap cavity ($\rho_o/z_o = 1.186$).

by

$$\gamma = \frac{\gamma_M}{1+\delta^2}, \tag{4.1}$$

where $\gamma_M$ is the maximum damping rate which occurs when the detuning $\delta$ (between the cyclotron and cavity mode resonance frequencies) is zero. The electron-

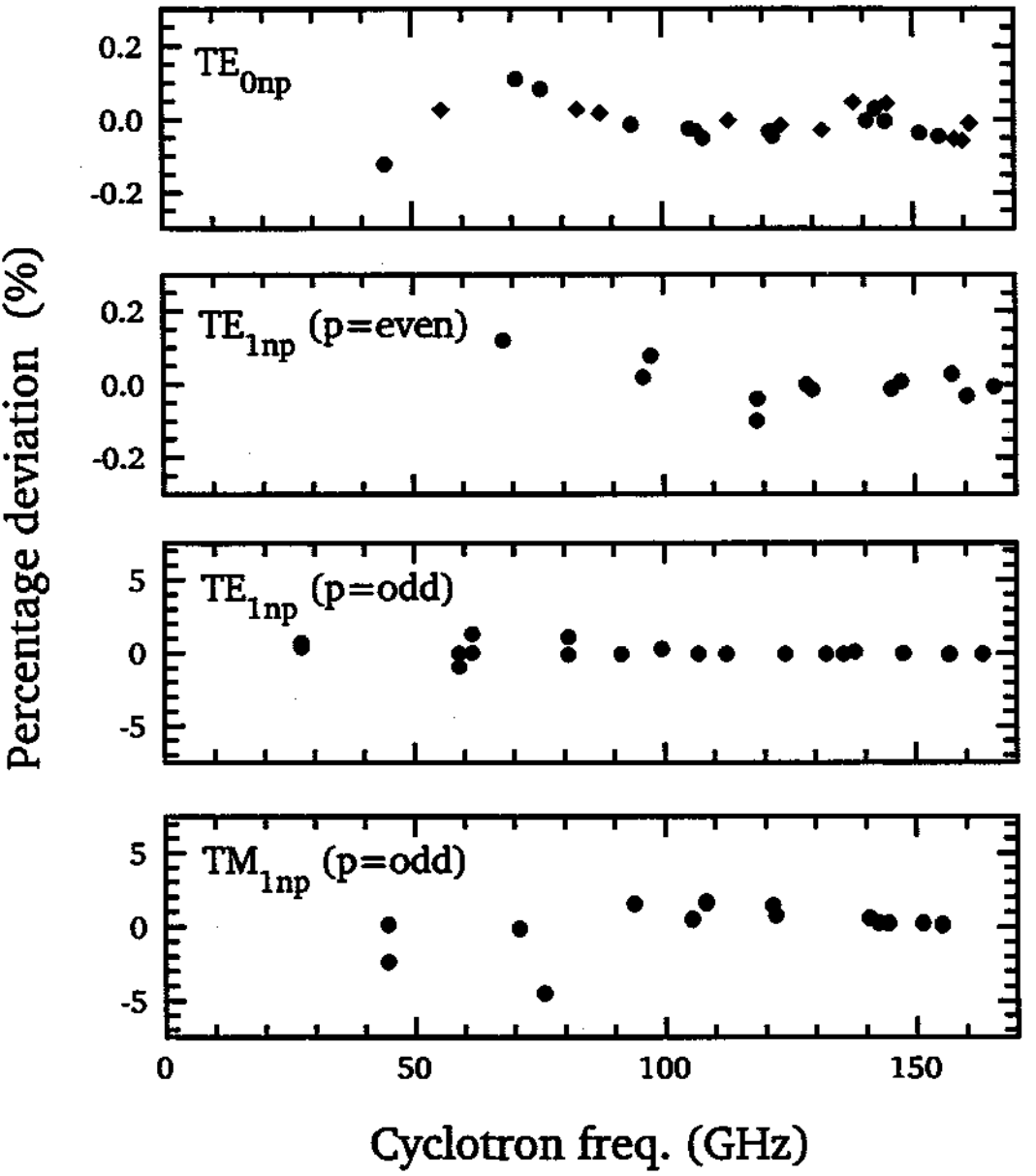


Figure 4.8: Comparison of observed and calculated eigenfrequencies for series of cavity modes of particular experimental interest.

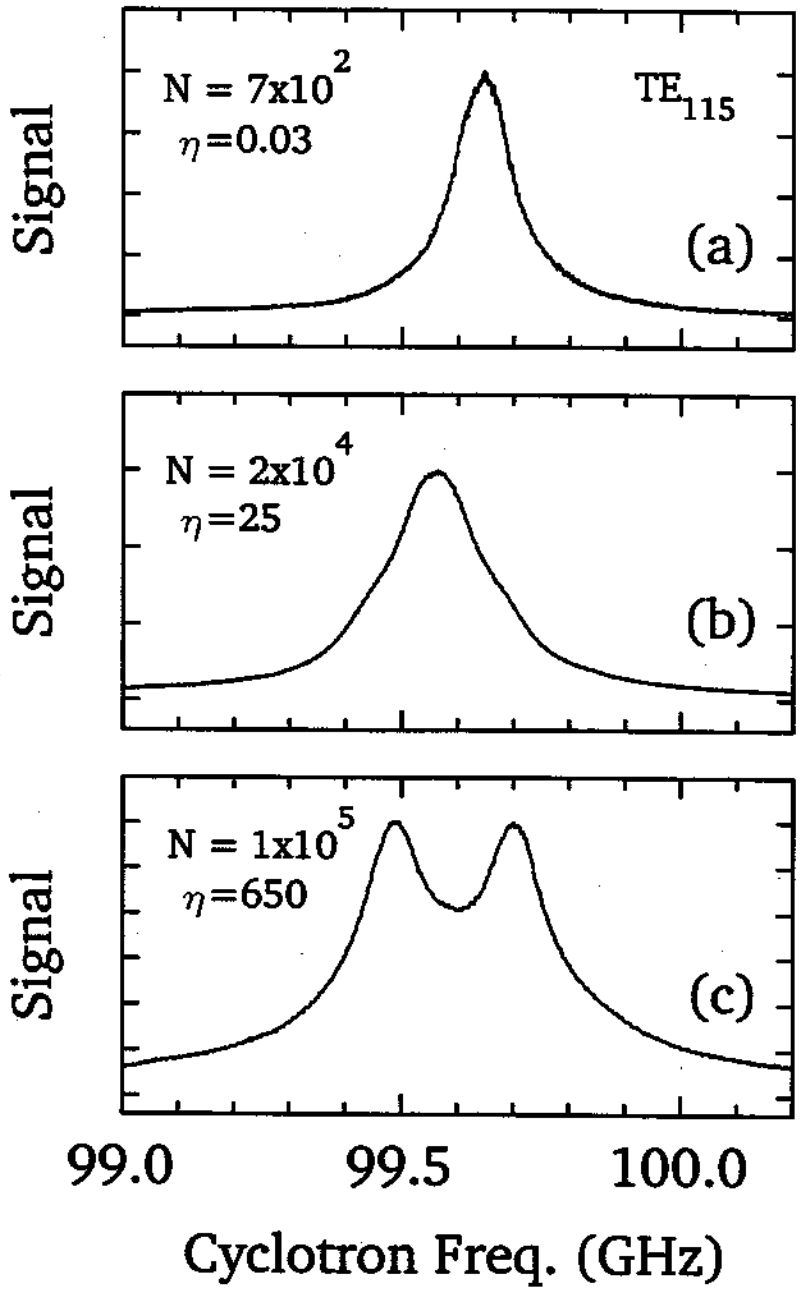


Figure 4.9: The Lorentzian lineshape (a) is modified to the strongly coupled lineshapes in (b) and (c) as the number of electrons $N$ is increased to increase the electron-cavity coupling.

cavity interaction is weak if the energy coupled into a cavity standing wave is dissipated in the cavity walls in a time shorter than is required for the cyclotron oscillator to re-absorb the energy. A useful parameter for comparing the coupling time between the CM cyclotron motion of N electrons and a cavity mode, on the one hand, to the decay rate of the standing wave itself due to losses in the cavity walls, on the other hand, is defined by

$$\eta = \frac{N^2 \gamma_M}{\Gamma_M}, \tag{4.2}$$

where the numerator gives the rate of energy transfer from the CM cyclotron motion to the $Mth$ cavity mode, and is proportional to $N^2$ because this rate depends on the square of the charge of the oscillator. The denominator $\Gamma_M$ gives the decay rate of energy in the cavity mode due to losses in the cavity walls. The weak coupling approximation which provides Eq. (4.1) is good for $\eta \ll 1$. Since the decay rate of one electron in free space is given by Eq. (1.3) and the quality factor $Q_M$ of the cavity mode is given by $\Gamma_M = \omega_M / Q_M$, we can rewrite $\eta$ defined in Eq. (4.2) as

$$\eta = \frac{4}{3}\left[\frac{\gamma_M}{Q_M \gamma_c}\right] N^2 Q_M^2 \left(\frac{r_e \omega_M}{c}\right), \tag{4.3}$$

in terms of known quantities (from calculations and measurements), with $r_e$ being the classical electron radius. The factor in square brackets is calculable, depending only on the geometry of the cavity, and is tabulated in Table 4.1.

We can make this coupling parameter $\eta$ rather large by either increasing $N$ or selecting a cavity mode with very high quality factor $Q_M$. The weak coupling approximation breaks down when $N$ or $Q_M$ is so large that the coupling time between an electron cloud and a cavity mode becomes shorter than the decay time for the energy in the cavity mode itself. Under this condition, the CM cyclotron oscillator and the cavity mode can form normal modes. For $TE_{115}$, we observe that $\nu_M = 99.84 GHz$ and $Q_M = 690$ in the weak coupling limit, and therefore

$$\eta = 6.51 \times 10^{-8}\ N^2. \tag{4.4}$$

With 700 electrons, $\eta = 0.03$ and a Lorentzian lineshape is observed, consistent

with Eq. (4.1). Broadening of the lineshape is observed (Fig. 4.9b, especially at its base) when $N = 2 \times 10^4$, which corresponds to $\eta = 25$. Evidence of normal-mode splitting is obtained (Fig. 4.9c) when the number of electrons is increased to $N = 10^5$, corresponding to $\eta = 650$. Normal-mode splitting has been observed recently in other systems with atoms coupled to a cavity mode as an atomic beam passes through a high-finesse optical cavity [71,97].

## 4.2 New Generation of g-2 measurements

As discussed in Sec. 1.2, the observation of inhibited spontaneous emission [32] and subsequent calculation of related shifts of the cyclotron frequency (See review in Ref. [37]) provided a serious obstacle to measurement of the magnetic moment of the electron and positron. Cavity shifts presently limit the precision of the measured magnetic moments of the electron and positron [88,89]. Inhibited spontaneous emission in the cyclotron motion has been observed in these experiments, with cyclotron decay time longer than in free space. The corresponding frequency shift which must be present (illustrated in Fig. 1.1b), however, has not been determined because the microwave properties of the hyperbolic trap are virtually unknown experimentally and are difficult to deal with even in principle. Consequently, latest measurements of the magnetic moment for the electron and positron

$$a(e^-) = 0.001\ 159\ 652\ 188\ 4\ (14)\ (40) \tag{4.5}$$

$$a(e^+) = 0.001\ 159\ 652\ 187\ 9\ (14)\ (44) \tag{4.6}$$

are reported with the largest uncertainty (40) due to cavity shifts [88,89]. This uncertainty, called the "most probable" cavity shift in the cyclotron frequency [88], was crudely estimated using our calculations for a cylindrical cavity model which is not a very satisfying approximation to a hyperbolic trap cavity.

QED calculations of the electron's anomalous magnetic moment have been pushed to nearly the same precision [53]. As mentioned earlier, however, QED relates measured $a$ values to measured values of the fine structure constant $\alpha$. For comparison to the measured $a$ values, the QED calculation and the measured fine structure constant together give an anomalous magnetic moment

$$a = 0.001\ 159\ 652\ 140\ 0\ (53)\ (41)\ (271). \tag{4.7}$$

The largest uncertainty (271) comes from uncertainty in the fine structure constant as measured using the quantum Hall effect. The uncertainties of (53) and (41) come from numerical calculations of the expansion coefficients $C_3$ and $C_4$ (not related to $\lambda_i$), respectively.

More precise tests of QED require improved precision for the measured fine structure constant first (this is expected), then improved measurements of $a$ and an improved QED calculation. It was pointed out to us by B.N. Taylor that

$$\alpha^2 = \frac{2R_\infty}{c}\frac{m(Na)}{m_p}\frac{m_p}{m_e}\frac{h}{m(Na)}. \tag{4.8}$$

The Rydberg constant $R_\infty$ is now known to within an uncertainty of $\sim 2 \times 10^{-10}$. Thus, an improved value of $\alpha$ can be obtained from precision measurements of the proton-electron mass ratio $m_p/m_e$ and the sodium-proton mass ratio $m(Na)/m_p$ in Penning traps, in combination with a proposed determination of $h/m(Na)$ (Planck's constant over mass of a sodium atom) using atomic interferometry[51]. The latest adjustment of fundamental constants is based in part on a somewhat more precise determination of $\alpha$ obtained by combining the QED calculation (assuming the exact validity of QED) with the measurement of $a$ to obtain

$$\alpha^{-1}(QED) = 137.\ 035\ 992\ 22\ (94). \tag{4.9}$$

The uncertainty in this QED determination of the fine structure constant is $7 \times 10^{-9}$ if the shift estimate turns out to be accurate.

### 4.2.1 Magnetic Moments Without Cavity Shifts

Controlling the interaction of an electron cyclotron oscillator with the cavity-modified vacuum will be crucial for higher precision tests of QED. Better $a$ measurements in trap cavities of unknown microwave properties appear difficult and unlikely. For example, using lossy materials as electrodes would make a hyperbolic trap cavity approximate the free-space vacuum (and thus avoid shifts due to unknown standing-wave fields). However, the cyclotron damping linewidth would also be as large as in free space, making precise frequency measurements more difficult. To relate the uncertainty $\Delta\omega_c$ in measuring the cyclotron frequency to the resulting uncertainty $\Delta a$ in the measured anomalous magnetic moment $a$, we note that

$$a = \frac{\omega_s - \omega_c}{\omega_c} \tag{4.10}$$

can be regarded as a definition of $a$, where $\omega_s$ is the electron's spin precession frequency. Since $a \approx 10^{-3}$ is small,

$$\frac{\Delta a}{a} \approx \frac{1}{a}\frac{\Delta\omega_c}{\omega_c}. \tag{4.11}$$

For $B = 5.9$ Tesla, without line splitting, the cyclotron frequency could therefore (in principle) be measured to $8\times10^{-12}$, from substitution of Eqs. (1.2) and (1.3) into Eq.(4.10). Setting $\Delta\omega_c$ equal to the free space line width yields $\Delta a/a \approx 8 \times 10^{-9}$. The experimental error currently quoted [88,89] is already much smaller than this free space linewidth.

The cylindrical cavity, with identified $p$ odd, $m = 1$ modes, is a greatly improved environment for experiments with a centered, one-electron cyclotron oscillator. To illustrate, a 10 GHz span of experimental interest is displayed in Fig. 4.10. Of the modes in this span, only $TM_{123}$ and $TE_{115}$ couple to the cyclotron motion of one electron at the center of the trap. $TE_{124}$, and $TE_{132}$ do not couple to one centered electron but are suited for sideband cooling of the axial motion. Both the damping rate $\gamma$ for an electron's cyclotron motion (for small enough damping

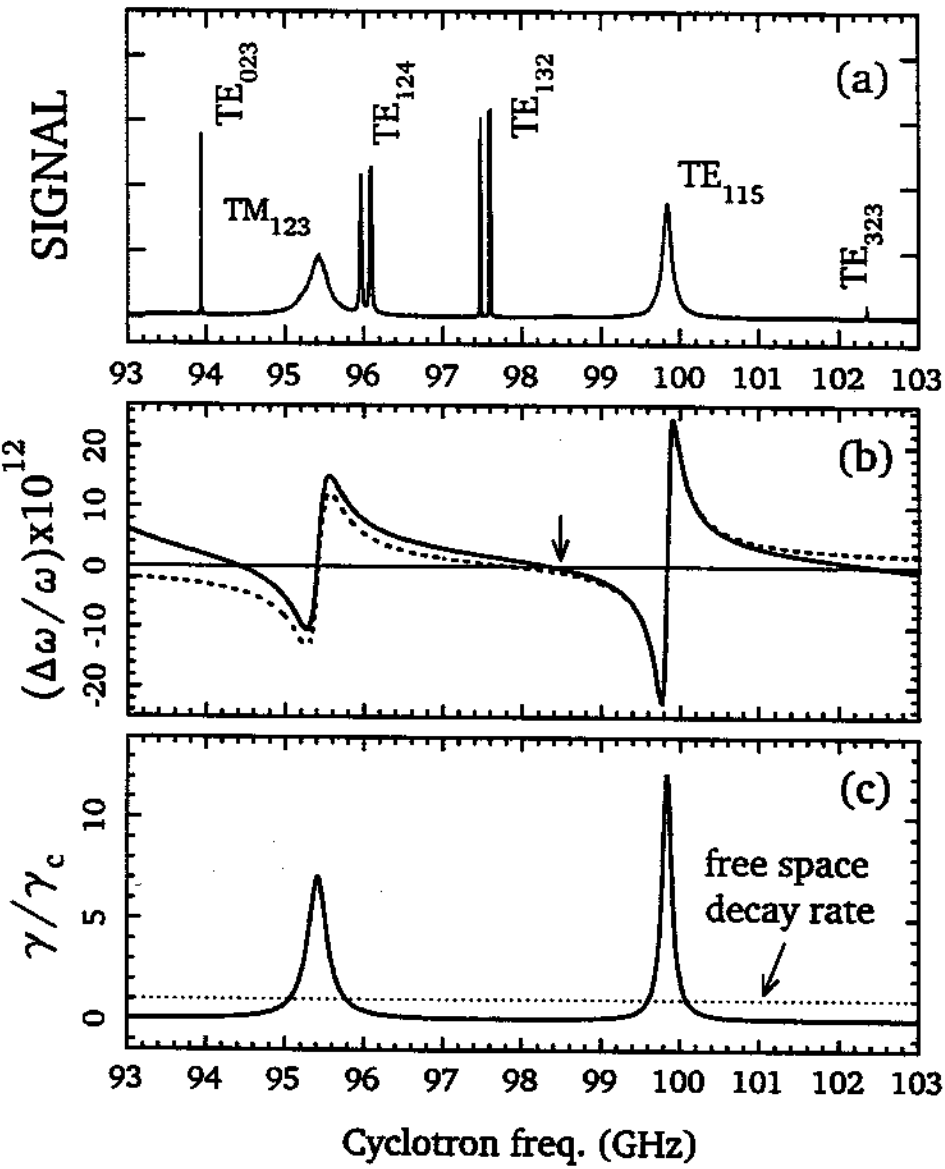


Figure 4.10: Observed cavity modes in a 10 GHz spectrum (a). Calculated frequency shifts (b) and damping rates (c) for one electron at the cavity center. The dashed line in (b) accounts for the two nearest modes that couple, $TM_{123}$ and $TE_{115}$. The solid line also includes the effect of nearby coupled modes not in this span.

[32]), and the cavity shift of its frequency $\Delta\nu$, could be measured as a function of $\nu_c'$ with one trapped electron, but this would take a very long time. However, to a good approximation, coupling to the Mth of these cavity modes (with resonant frequency $\nu_M$) yields the explicit forms [37]

$$\gamma = A_M \frac{Q_M}{1+(Q_M\delta_M)^2} \tag{4.12}$$

$$2\pi\Delta\nu = \frac{1}{2}A_M\frac{(Q_M)^2\delta_M}{1+(Q_M\delta_M)^2} = \frac{1}{2}\gamma Q_M\delta_M. \tag{4.13}$$

The constants $A_M$ are precisely known (equivalent to those tabulated [37] as elaborated in Sec. 4.4) because the field configurations of these modes are known. Both $\gamma$ and $\Delta\nu$ are functions of the "detuning" $\delta_M = 2(\nu_c' - \nu_M)/\nu_M$ (which is accurately controlled and measured) and the quality factor for the mode $Q_M$. These explicit forms, with $\nu_M$ and $Q_M$ from the measurements described earlier (summing over nearby modes as necessary and including manageable renormalization corrections neglected here [37]) can be used to compute the frequency shift (Fig. 4.10b) and damping rate (Fig. 4.10c) for a centered electron. The hope is to compare with several specific measurements with one electron and then to deduce the cyclotron frequency (i.e. the magnetic field) at which the electron's cyclotron frequency is not shifted by the cavity (arrow in Fig. 4.10b ). The damping width is 50 times narrower than in free space at this unshifted cyclotron frequency. The likelihood for thereby improving the measurement accuracy is very high.

### 4.2.2 Rapid Control of Electron-Cavity Coupling

The simple standing wave pattern of $m = 1$ modes can be used to change the cyclotron damping rate rapidly without changing the magnetic field (which would take months to restabilize sufficiently for high precision experiments). This is possible because the coupling between the cyclotron oscillator and a cavity mode vanishes at a node of the standing wave. An electron can be moved up and down by by adding an anti-symmetric electric potential $V_A$ across the endcaps

(Fig. 4.11a). Fig. 4.11b represents the magnitude of a component of the transverse electric field of a $TE_{1n3}$ mode along the z-axis. If an electron is displaced from the center of the trap (where its coupling with the cavity mode is strongest) along the z-axis by a quarter wavelength to the nearest node, then its interaction with the standing-wave is switched off.

Electronic control of the electron-cavity coupling is demonstrated in Fig. 4.12. The peak in Fig. 4.12a is due to coupling of $TE_{027}$ to an electron cloud near the trap center. $TE_{027}$ has 7 anti-nodes between the endcaps, with $\lambda/4 = 550\ \mu$m. For Fig. 4.12b, the electron cloud is displaced by 510 $\mu$m from the trap center along its axis. Proximity to the node causes the resonant peak in Fig. 4.12a to disappear. Instead, a pair of peaks separated by $2\omega_z$ appear in the spectrum because the

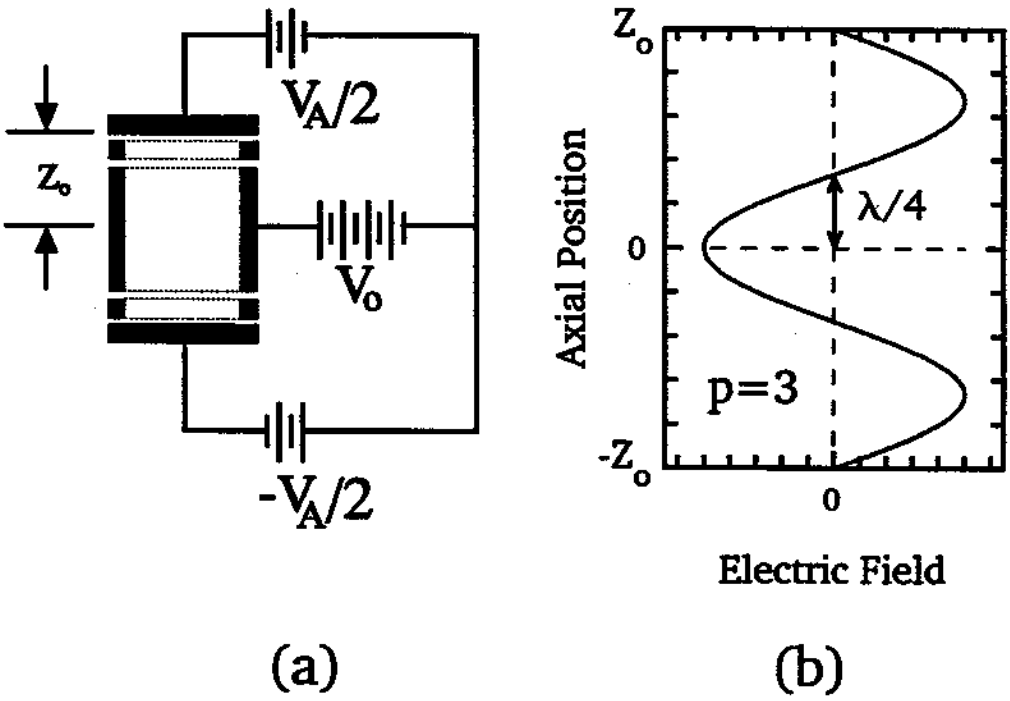


Figure 4.11: (a) Antisymmetric potential across endcaps displaces electrons along the z-axis. (b) Representation of transverse electric field component near the z-axis for a p=3 mode.

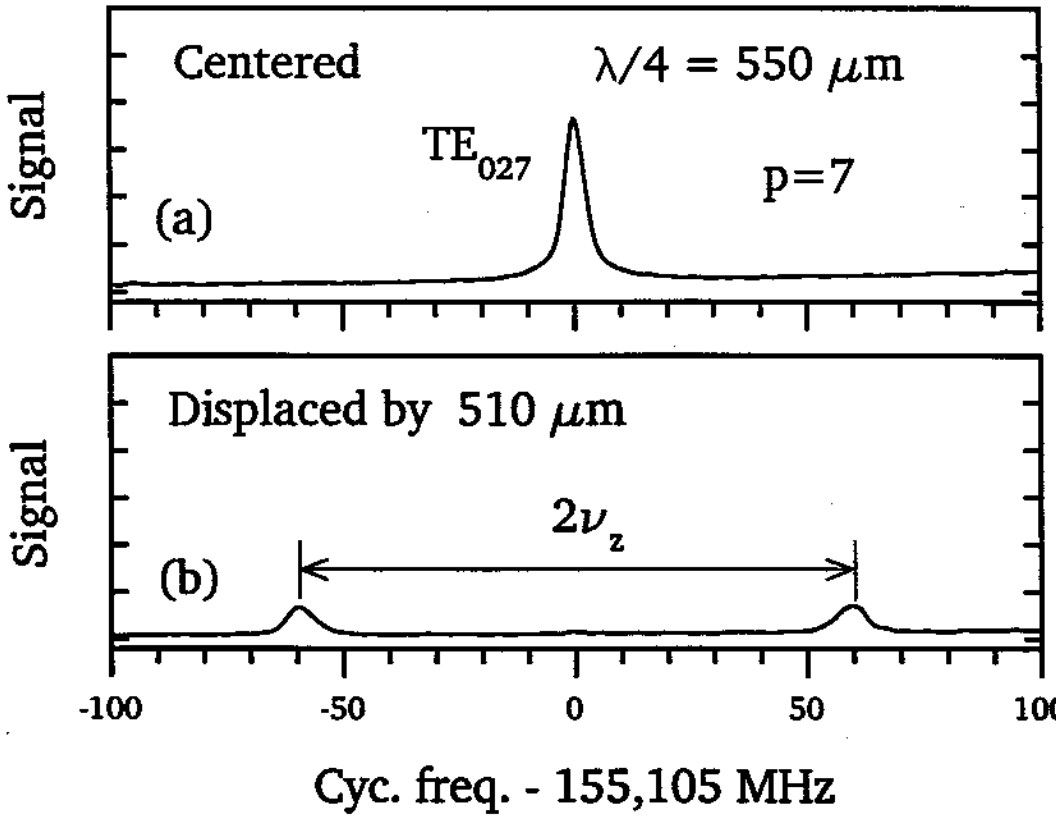


Figure 4.12: (a) Observed resonance for $TE_{027}$ ($\lambda/4 = 550\mu$m) with a centered electron cloud. (b) Motional doublet observed when the electrons are displaced from the center by $\Delta z = 510\mu$m.

electrons are oscillating at frequency $\omega_z$ through the node plane at $z \approx \lambda/4$ .

### 4.2.3 Sideband Cooling of Axial Motion

The axial motion of a trapped electron is dissipated as Joule heating in a resistor connected between appropriate electrodes, cooling the axial motion into thermal equilibrium with the resistor. Even at 4 K, thermal axial motions are highly undesirable in efforts to study the relativistic, quantum structure of the cyclotron

oscillator because the thermal energy is coupled into the cyclotron motion via several mechanisms.

To bring the axial motion to a much lower temperature, the electron would be decoupled from the resistor and a sideband cooling technique [94,10] would be employed. Modes with even $p$ and $m = 1$ (eg. in Fig. 4.10), when driven at $\nu_c' - \nu_z$, produce the proper oscillatory spatial gradients required to transfer the axial energy into the cyclotron motion. The cyclotron excitation, in turn, dissipates the transferred thermal energy into the cavity via modes with odd $p$ and $m = 1$. It should be possible to cool the undamped axial motion to an extremely low temperature limit [10]

$$T_z = (\nu_z/\nu_c')T_c. \tag{4.14}$$

With the frequencies used here, this would be an unprecedented (and extremely useful) axial temperature of 2 mK for $T_c = 4.2K$. Because the field intensity builds up within the high Q cavity, much less drive power should be required than was estimated for propagating plane-waves [10]. These same modes have a transverse magnetic field at the cavity center and could thus be used to directly flip an electron spin (when driven at $\omega_s$). Off-resonance cyclotron excitations by the strong spin flip drive are suppressed because these modes do not couple directly to the cyclotron motion.

## 4.3 Calibrating the Monitored Currents

The cyclotron frequency is swept by ramping the current in a superconducting solenoid which provides the magnetic field, as already described. The current $I$ supplied to the superconducting magnet by a regulated power supply is monitored, digitized and stored in a computer at a rate of $\sim 3$ data points per second. The frequency of the cyclotron oscillator at any time is, using Eq. (2.10),

$$\nu_c = \frac{e}{m}B_z(t) = \frac{e}{m}g\left(I - \frac{V}{L}\tau_o\right), \tag{4.15}$$

where $e/m$ is the charge-to-mass ratio of an electron. The constant $\tau_o$ takes into account the current drawn by the protection resistor shunting the superconducting solenoid. By sweeping the current from 0 to 40 Amperes, the cyclotron oscillation frequency is varied between 0 and 167 GHz. This maximum frequency corresponds to the maximum field for the superconducting solenoid. The conversion from monitored current to the cyclotron frequency is measured accurately by using a high precision microwave source to drive the cyclotron oscillator. For the superconducting solenoid used to obtain Fig. 4.3, the driven resonant frequency $\nu_c$ at a known current $I$ gives

$$\frac{\nu_c}{I} = 4.1854(2)\text{GHz/A} \quad . \tag{4.16}$$

The uncertainty is due to the statistical error in current measurement. This is in good agreement with the theoretical value calculated from the windings of the solenoid, within the tolerance of the solenoid and the calibration error of the metering resistor.

To measure the offset constant $\tau_o$, we choose a high Q cavity mode. The axial CM energy of a synchronized electron cloud is maximum when the cyclotron oscillation is in resonance with the cavity mode, shown in Fig. 4.13(a). The current corresponding to the cavity mode resonance, $I_N$, is measured for various sweep rates. The sweep rate $V/L$ is measured from the time-stamped, digitized record of current readings (see, e.g., Fig. 2.6). The linear variation of the resonant current, $I_N$, with the sweep rate $V/L$ is shown in Fig. 4.13(b). The slope directly gives

$$\tau_o = 101(1)\text{s} \quad , \tag{4.17}$$

which characterizes the shunt resistor across the superconducting solenoid mentioned earlier.

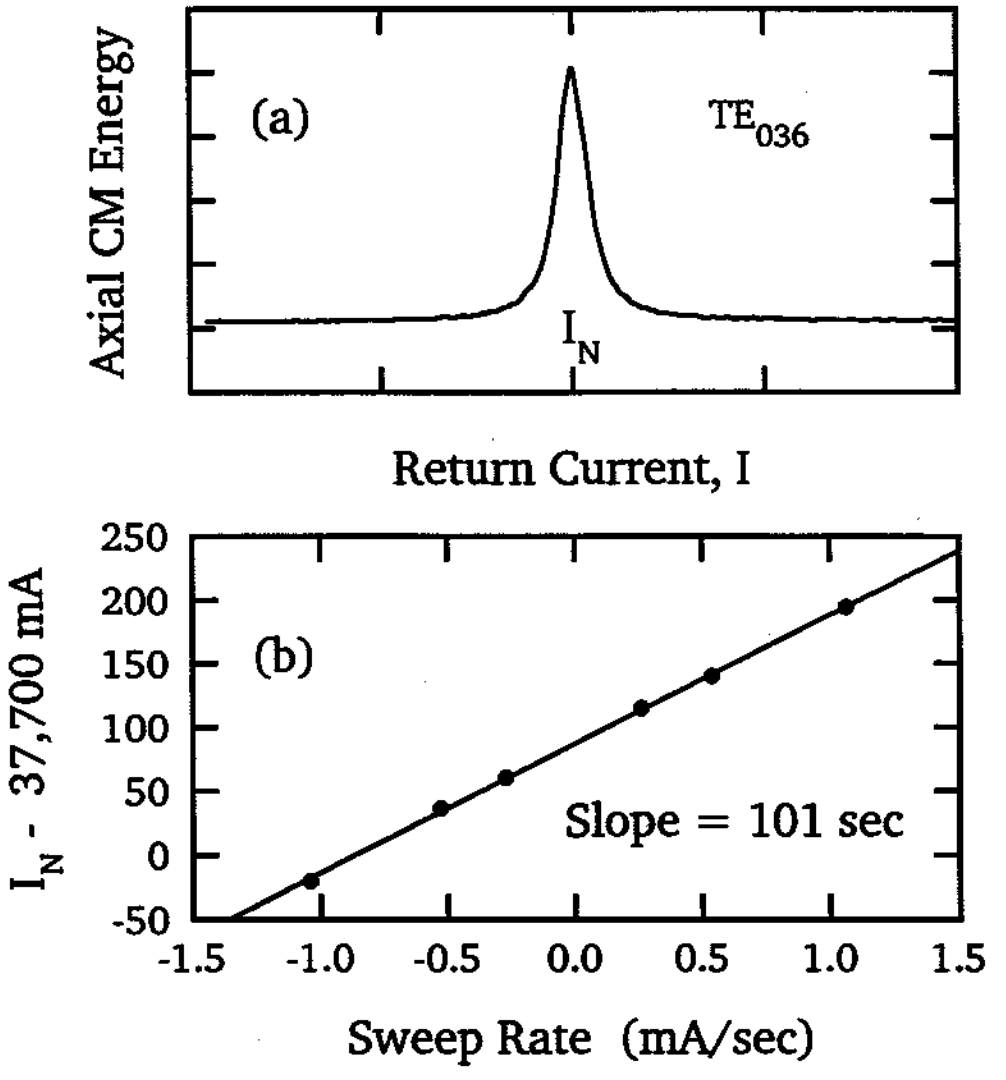


Figure 4.13: (a) Cavity mode resonance for field calibration. (b) Measurement of offset constant $\tau_o$

## 4.4 Electron-Cavity Interactions

The dynamics of one cyclotron oscillator localized in the midplane (near the center) of a cylindrical, microwave cavity is governed by [8,9]

$$m\dot{\mathbf{v}} - (e/c)\mathbf{B} \times \mathbf{v} = e\mathbf{E}^T \quad , \tag{4.18}$$

where $\mathbf{v} = \dot{\rho}$ is the velocity in the midplane. The transverse electric field $\mathbf{E}^T$, in the dipole approximation, is due to radiation standing-wave modes with $m = 1$ (i.e., $TE_{1np}$ and $TM_{1np}$), generated as the accelerating electron radiates into the

cavity. Thus Eq. (4.18) indicates that the cavity standing waves act back upon the cyclotron oscillator. The calculations are classical since it has been shown that within a high level of accuracy, the exact apparatus of quantum electrodynamics yields the classical results [4].

The essential features of this interaction are also contained in a simpler electromechanical model (Fig. 2.13) appropriate when one cavity mode is considered [3]. In this model, the selected $M^{th}$ cavity mode is represented by a series LCr tuned circuit. Such a tank circuit is resonant at angular frequency $\omega_M = (LC)^{-1/2}$ with damping width $\Gamma_M = r/L$. The electron oscillator is represented as a charge $e$ and mass $m$ on a spring with spring constant $m(\omega_c')^2$. The electron oscillation $z(t)$ excites a current $\dot{Q}(t)$ in the tuned circuit. The oscillating current in the tuned circuit, in turn, produces an RF electric field which acts back on the electron. The interaction potential for these two coupled oscillators is given by

$$V_{int} = -\left[\frac{\kappa q}{2z_o C}\right] z(t)\, Q(t), \tag{4.19}$$

where the dimensionless coupling $\kappa = 1$ for a capacitor with infinite parallel plates (separated by $2z_o$). Using familiar Lagrangian equations, we find that, analogous to Eq. (4.18),

$$m\left[\frac{d^2}{dt^2} + (\omega_c')^2\right] z(t) = -\left[\frac{\kappa q}{2z_o C}\right] Q(t). \tag{4.20}$$

The excitation of the tuned circuit is described by

$$L\left[\frac{d^2}{dt^2} + \Gamma_M \frac{d}{dt} + (\omega_M)^2\right] Q(t) = -\left[\frac{\kappa q}{2z_o C}\right] z(t). \tag{4.21}$$

We can neglect Johnson noise (which represents the 4 K radiation of the cavity in thermal contact with the liquid helium bath).

In the weak-coupling regime (wherein the cavity field decays due to wall losses in a time shorter than required for the electron to re-absorb the radiation), the tuned circuit effectively damps the electron oscillation $z(t)$ at rate $\gamma$ and shifts its resonant frequency to $\tilde{\omega}_c'$. Since the cavity modes typically have high quality

factors ($Q \sim 10^3$ or higher), the damping and frequency shift take the simple forms

$$\gamma = \gamma_M \frac{1}{1+\delta^2} , \tag{4.22}$$

$$\tilde{\omega}_c' - \omega_c' = \frac{1}{2}\gamma_M \frac{\delta}{1+\delta^2} . \tag{4.23}$$

In terms of the effective resistance $R = L/(rC)$, the maximum damping rate $\gamma_M$ is given by

$$\gamma_M = \left[\frac{\kappa q}{2z_o}\right]\frac{R}{m}. \tag{4.24}$$

The resonant frequencies of the tuned circuit and electron motion are $\omega_M$ and $\omega_c$, respectively, when the interaction is turned off. The unperturbed resonance frequency of the two oscillators are related by a detuning $\delta$ defined by

$$\omega_c' = \omega_M + \frac{1}{2}\Gamma_M\delta. \tag{4.25}$$

If the electron oscillator and the LCr circuit are tuned to the same unperturbed resonance frequency (i.e. $\delta = 0$) there is no frequency shift, but the damping rate is maximum. When $\delta \neq 0$, the damping rate is reduced but the resonant frequency of the electron oscillator is shifted. The maximum frequency shifts $\pm\gamma_M/4$ occur near resonance, at detunings $\delta = \pm 1$. The characteristic shapes for $\gamma$ and $\Delta\omega$ are shown in Fig. 1.1 and are clearly evident in more detailed calculations.

Since $\gamma_M \sim R \sim Q_M$, the maximum damping and maximum frequency shift are larger when the quality factor $Q_M = \omega_M/\Gamma_M$ is larger. To display the Q dependence explicitly we write

$$\frac{\gamma_M}{\omega_M} = 2Q_M\left(\frac{\lambda_M}{\omega_M}\right)^2 \tag{4.26}$$

thereby defining the coupling strength $\lambda_M$ [98]. This definition also allows the use of a simple form for the electron's frequency shift and damping rate

$$\Delta\omega - i\frac{\gamma}{2} = \frac{\omega(\lambda_M)^2}{\omega^2 + i\omega\Gamma_M - \omega_M^2} , \tag{4.27}$$

which can be generalized to include interactions with more than one cavity mode by summing the right hand side over the mode index $M$.

For Eq. (4.27) and its generalization to be quantitatively useful, the coupling constants $\lambda_M^2 = \lambda_{n,l}^2$ have been calculated for regular cavities of interest [37]. In particular, for the cylindrical cavity, the mode index $M$ is identified here with the two quantum numbers $n = 0, 1, 2, ...$ and $l = 1, 2, 3, ....$ When the magnetic field is along the symmetry axis of the cavity, these two indices identify the subset of cavity modes which couple to a cyclotron oscillator located at the center of the cavity. Two types of modes couple to the cyclotron motion and for both it is convenient to use $k_n = (n + 1/2)\pi/z_o$. For TE (transverse electric) modes

$$\lambda_{n,l}^2 = \frac{r_e c^2}{z_o \rho_o^2} \frac{2}{\alpha_l^2 - 1} \frac{\alpha_l^2}{J_1(\alpha_l)^2} \tag{4.28}$$

$$\omega_{n,l}^2 = \left( k_n^2 + \frac{\alpha_l^2}{\rho_o^2} \right) c^2 \tag{4.29}$$

where $\alpha_l$ (defined by $J_1'(\alpha_l) = 0$) is the $l^{th}$ zero of the derivative of the first-order Bessel function. For TM (transverse magnetic) modes which couple to electron cyclotron motion

$$\lambda_{n,l}^2 = \frac{r_e c^2}{z_o \rho_o^2} \frac{2 k_n^2 c^2}{\omega_{n,l}^2} \frac{1}{J_0(\beta_l)} \tag{4.30}$$

$$\omega_{n,l}^2 = \left( k_n^2 + \frac{\beta_l^2}{\rho_o^2} \right) c^2 \tag{4.31}$$

where $\beta_l$ (given by $J_1(\beta_l) = 0$) is the $l^{th}$ zero of the first order Bessel function. The quantum numbers $n$ and $l$ which we use to label the cavity modes which couple to the electron are simply related to common conventions for labeling all the modes of a cylindrical cavity. For example, in the textbook by Jackson [49] the origin of the coordinate system is translated to the center of the bottom endcap , and the TE and TM modes identified above are labeled as $TE_{1,l,2n+1}$ and the $TM_{1,l,2n+1}$, respectively. Couplings for other cavity geometries of interest are found in an earlier work [37].

Unfortunately, the simple theory is afflicted with problems arising from self-field interaction. To see this, we note that the standing wave field is actually composed of two contributions

$$\mathbf{E}^T = \mathbf{E}_{self} + \mathbf{E}', \tag{4.32}$$

the self-field $\mathbf{E}_{self}$ radiated directly by the oscillator (as if into free space) and the reflected field $\mathbf{E}'$ which is reflected from the cavity walls. The back reaction of a self-field upon the accelerating charge which is radiating, is well known to lead to difficulties and divergences in classical electricity and magnetism [69] (inherited by QED in addition to divergences of its own). In our particular situation, the real part of the mode sum

$$\Delta\omega - i\frac{\gamma}{2} = \omega - \omega_c - i\frac{\gamma_c}{2} = \omega \sum_M \frac{\lambda_M^2}{\omega^2 + i\omega\Gamma_M - \omega_M^2}, \tag{4.33}$$

diverges when the sum includes all the cavity modes. For a correctly renormalized calculation, the self-field term is replaced by a radiation damping term for radiation into free space (with damping rate $\gamma_c$) and only the transverse reflected field $\mathbf{E}'$ acts back upon the cyclotron oscillator, so that Eq.4.18) is rewritten as

$$\dot{\mathbf{v}} - \omega_c \times \mathbf{v} + (\gamma_c/2)\mathbf{v} = (e/m)\mathbf{E}'. \tag{4.34}$$

Only in special cases is it possible to separate the reflected field and the self-field which together make up the standing wave. The high degree of symmetry for a spherical cavity [11,20] makes the removal of the self-field relatively simple because the free-space radiation from the oscillator at the center contains only outgoing spherical waves, easily distinguished from the reflected waves. A cylindrical cavity [8,9] has less symmetry, but the separation can still be accomplished by using image charges to satisfy the cavity boundary conditions. The reflected field is thus clearly distinguished as the field of the images. For a hyperbolic cavity (which corresponds to the trap within which the electron's magnetic moment was measured) a separation of self and reflected fields is completely intractable. Finite mode sums as done in the simple model are the only possibility. Comparisons of a modified mode sum and a complete calculation for the cylindrical cavity are used to estimate the optimal number of terms to be included in the finite mode sum, even though the mode density is significantly higher in a hyperbolic cavity.

The usefulness of the simple theory is limited especially when the electron cyclotron oscillator is not near to resonance with a high Q cavity mode. A detailed discussion of how the divergences arise and can be partially circumvented

in this model has been presented [12,37]. In general, the contribution from any off-resonant ($M^{th}$) mode to the frequency shift $\Delta\omega$ of the electron oscillator, going as $\frac{1}{2}(\lambda_M)^2/(\omega_c - \omega_M)$, independent of $Q_M$ is overstated slightly due to self-field in the standing wave. The overstated contributions add up as the contributions from many modes are included. Optimal use of the simple, mode sum model thus requires a careful choice of the number of cavity modes included in the sum. Beyond a certain number of terms, the real part of the mode sum will start to diverge. Eventually, the mode sum over an infinite number of such small contributions diverges. It is difficult to establish the optimum number of terms or the accuracy of the truncated mode sum except by comparison to a calculation which avoids the divergences entirely [12]. A modified mode sum formula was obtained [12] which converges for the case of a cylindrical cavity and can be used to obtain the unshifted cyclotron frequency to 1 part in $10^9$.

## 4.5 Full Spectrum Below 166 GHz

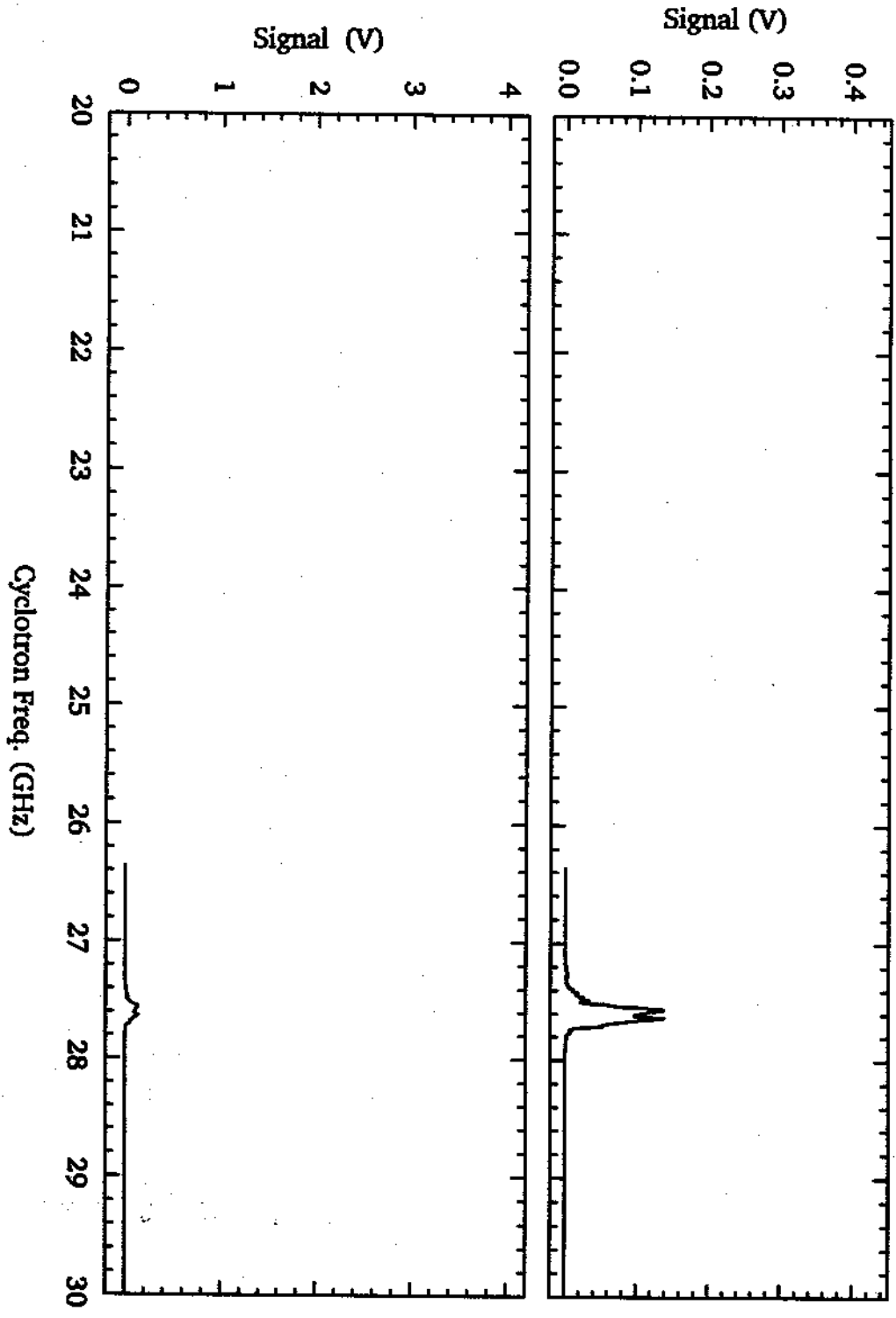


Figure 4.14: Observed cavity modes below 166 GHz.

## 4.5 Full Spectrum Below 166 GHz

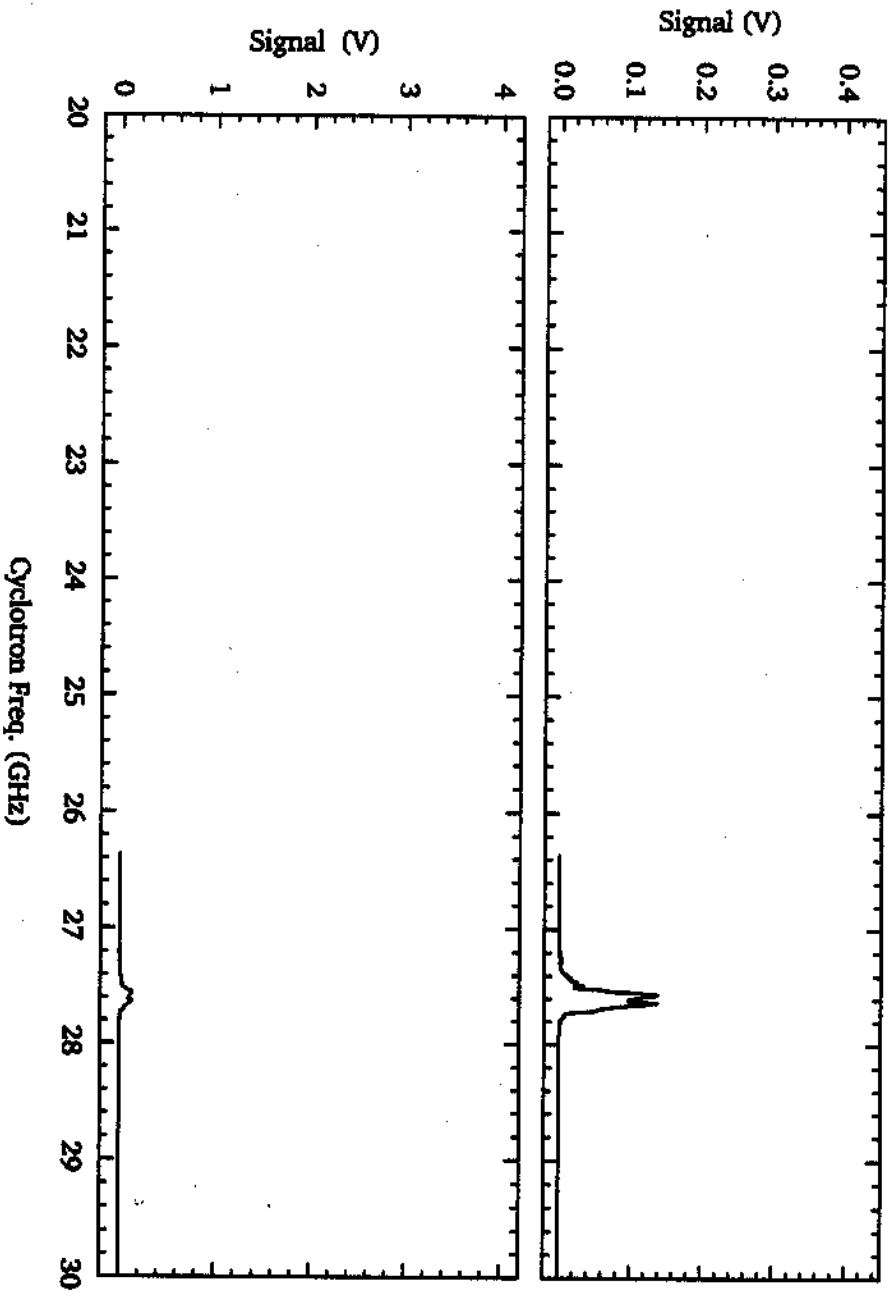


Figure 4.14: Observed cavity modes below 166 GHz.

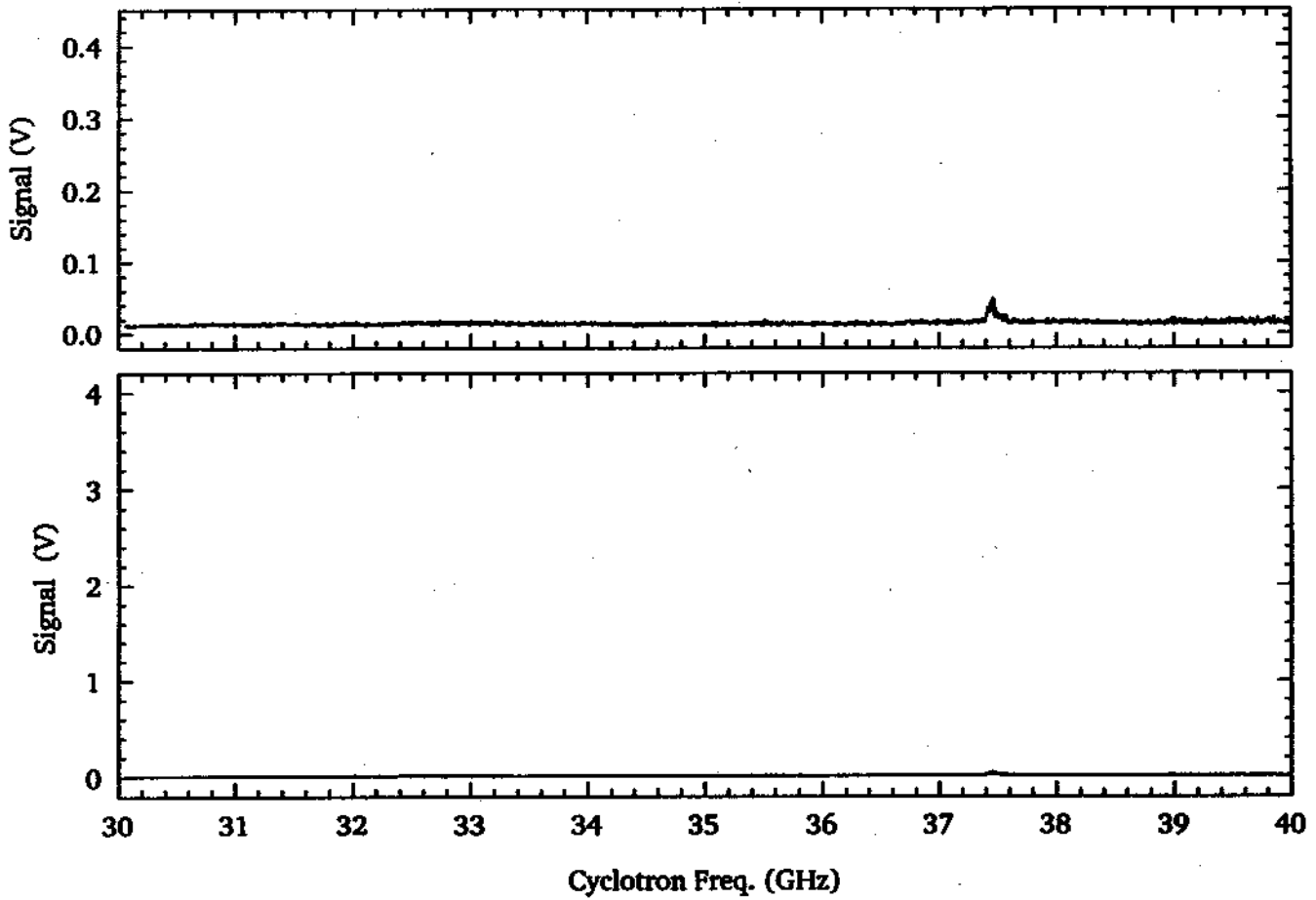
Signal (V)
0.4
0.3
0.2
0.1
0.0
Signal (V)
4
3
2
1
0
30
31
32
33
34
35
36
37
38
39
40
Cyclotron Freq. (GHz)

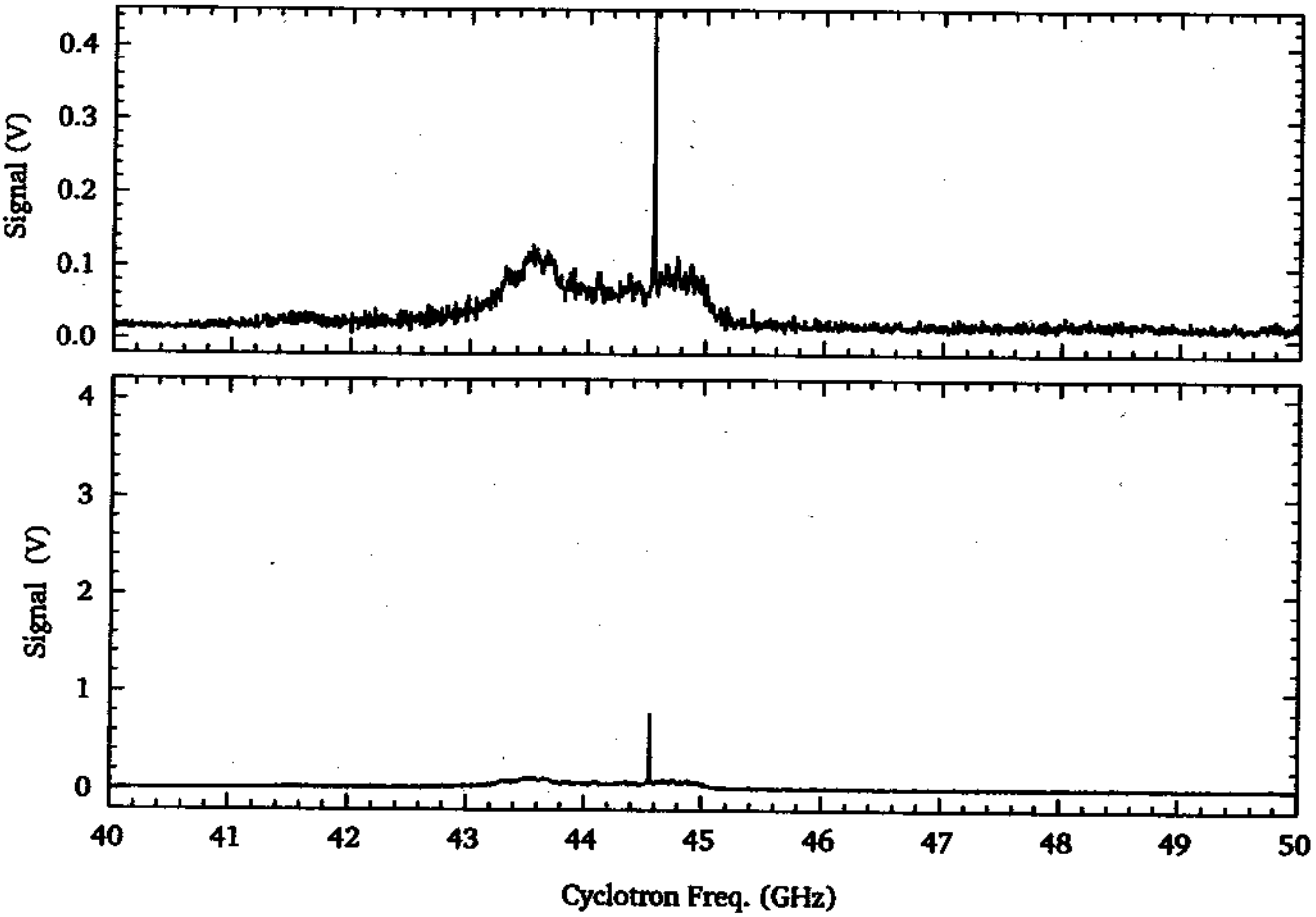
0.4
0.3
0.2
0.1
0.0
Signal (V)
4
3
2
1
0
Signal (V)
40
41
42
43
44
45
46
47
48
49
50
Cyclotron Freq. (GHz)

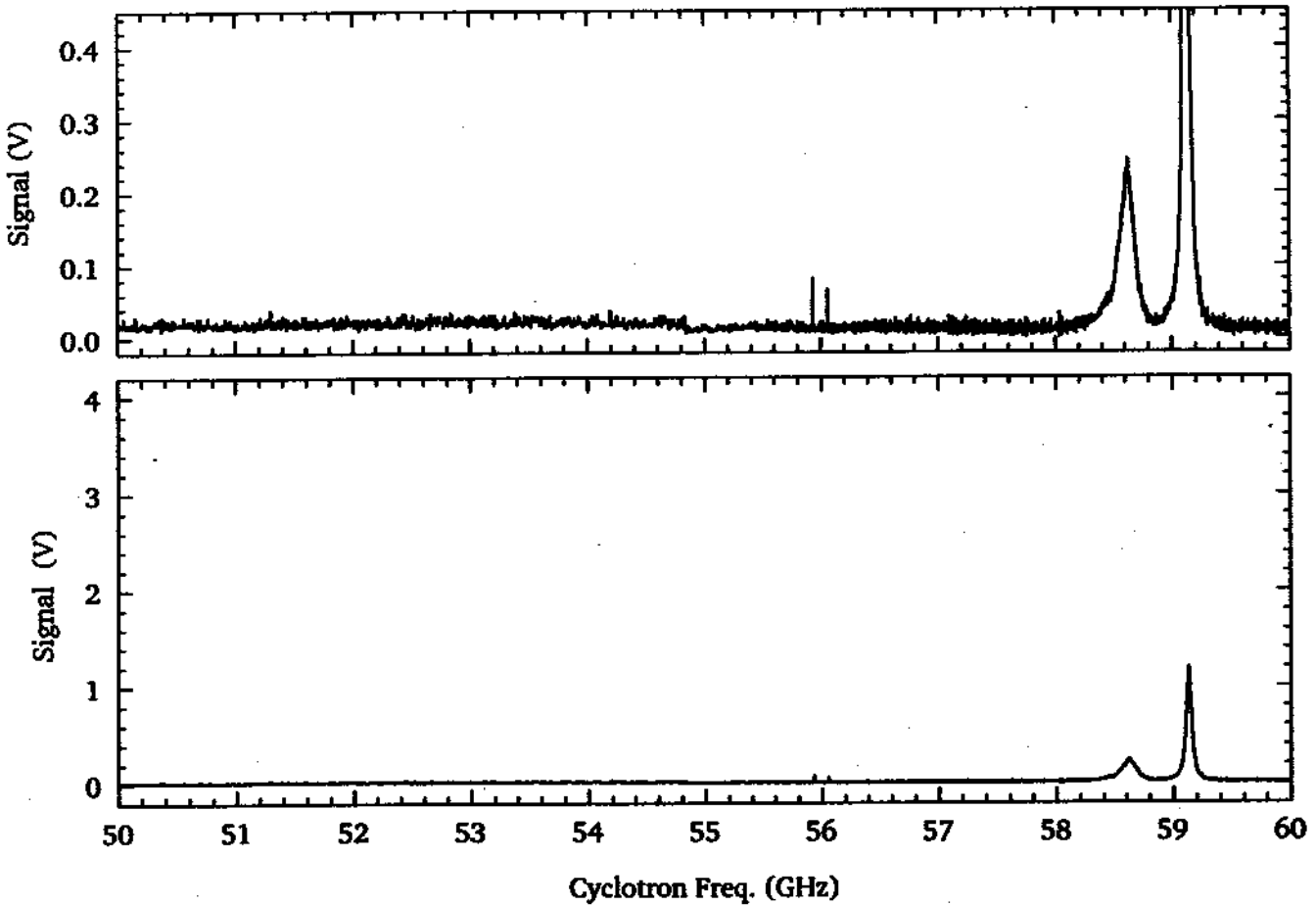
Signal (V)
0.4
0.3
0.2
0.1
0.0
Signal (V)
4
3
2
1
0
50
51
52
53
54
55
56
57
58
59
60
Cyclotron Freq. (GHz)

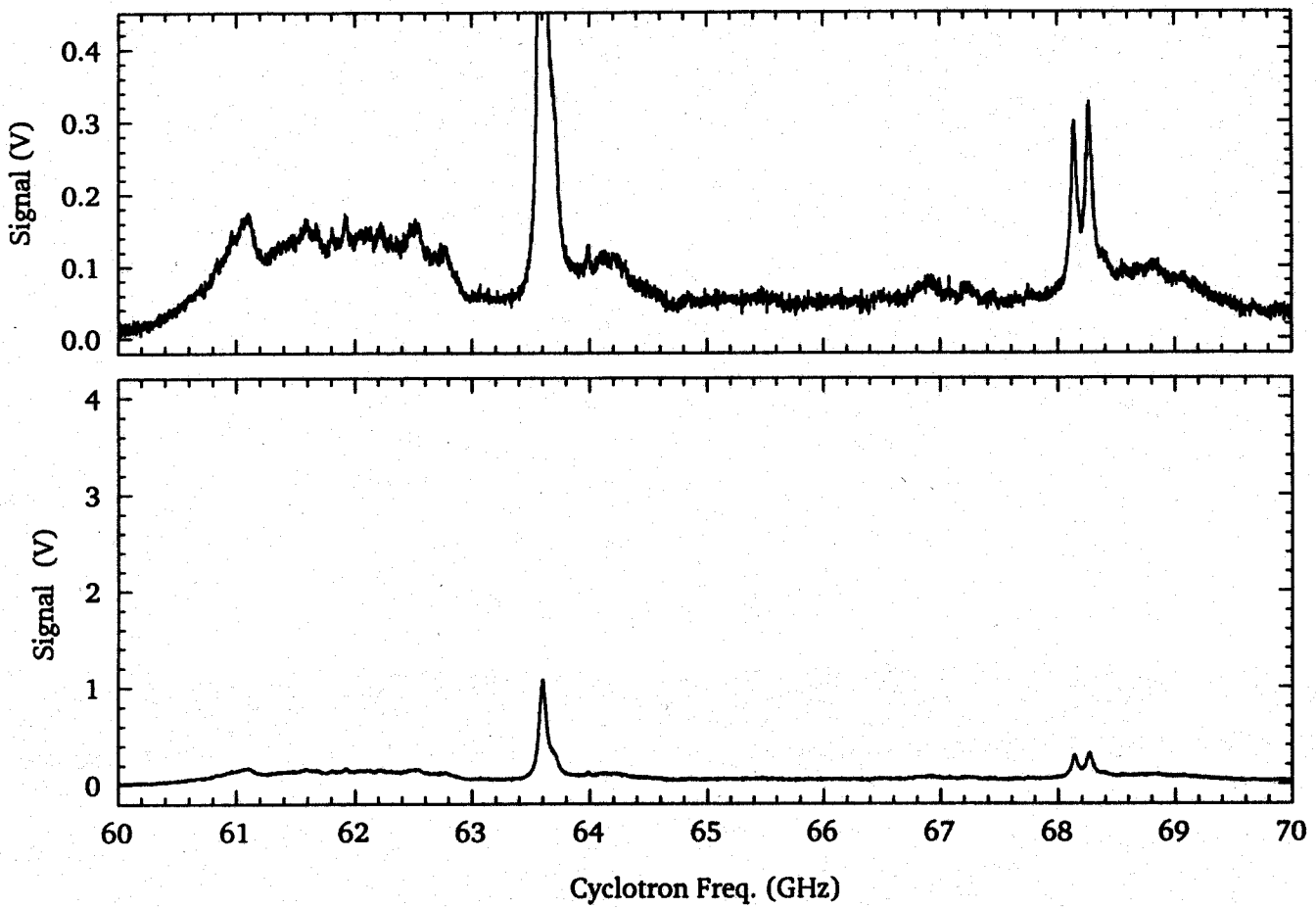
Signal (V)
0.4
0.3
0.2
0.1
0.0
Signal (V)
4
3
2
1
0
60
61
62
63
64
65
66
67
68
69
70
Cyclotron Freq. (GHz)

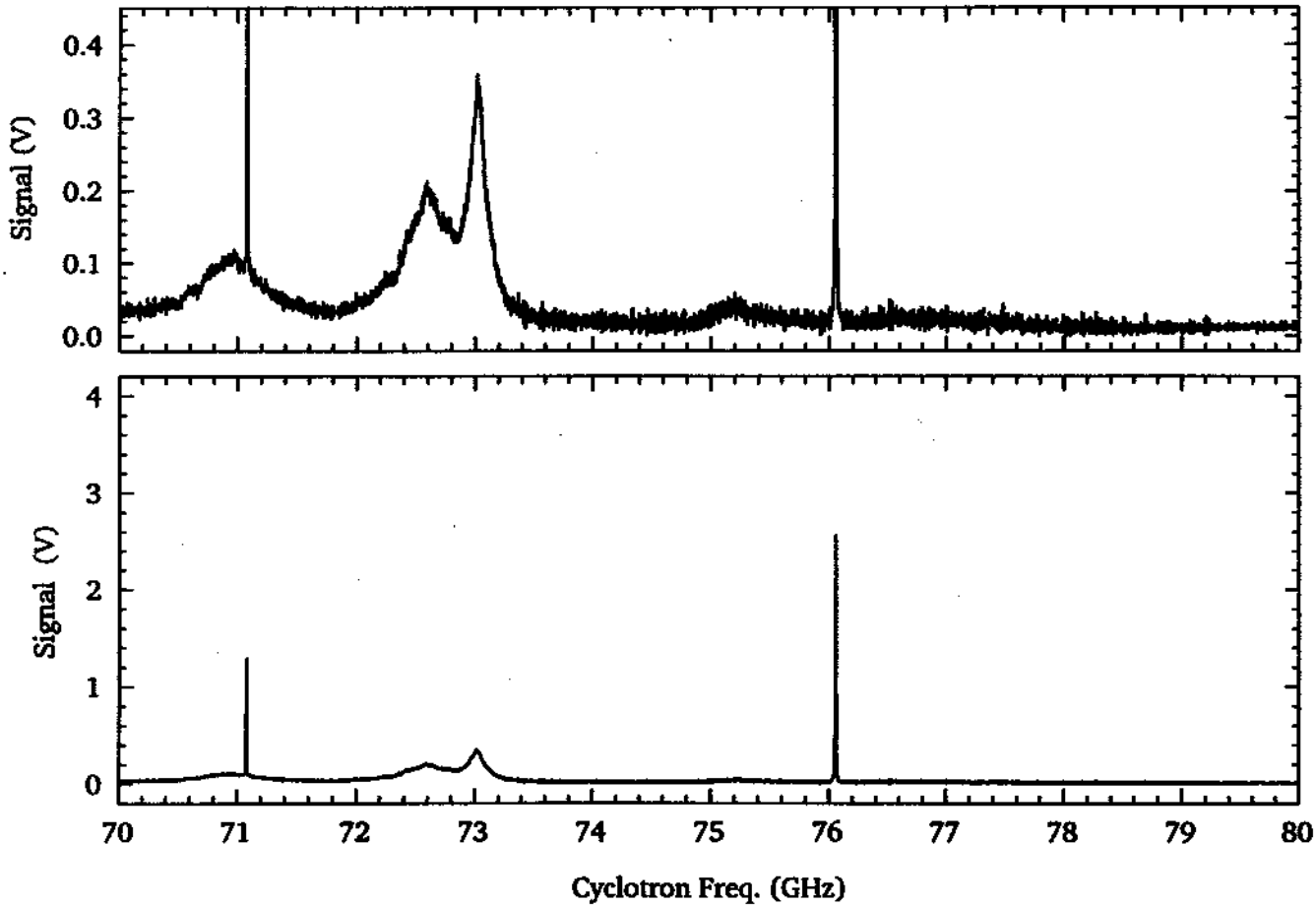
Signal (V)
0.4
0.3
0.2
0.1
0.0
Signal (V)
4
3
2
1
0
70
71
72
73
74
75
76
77
78
79
80
Cyclotron Freq. (GHz)

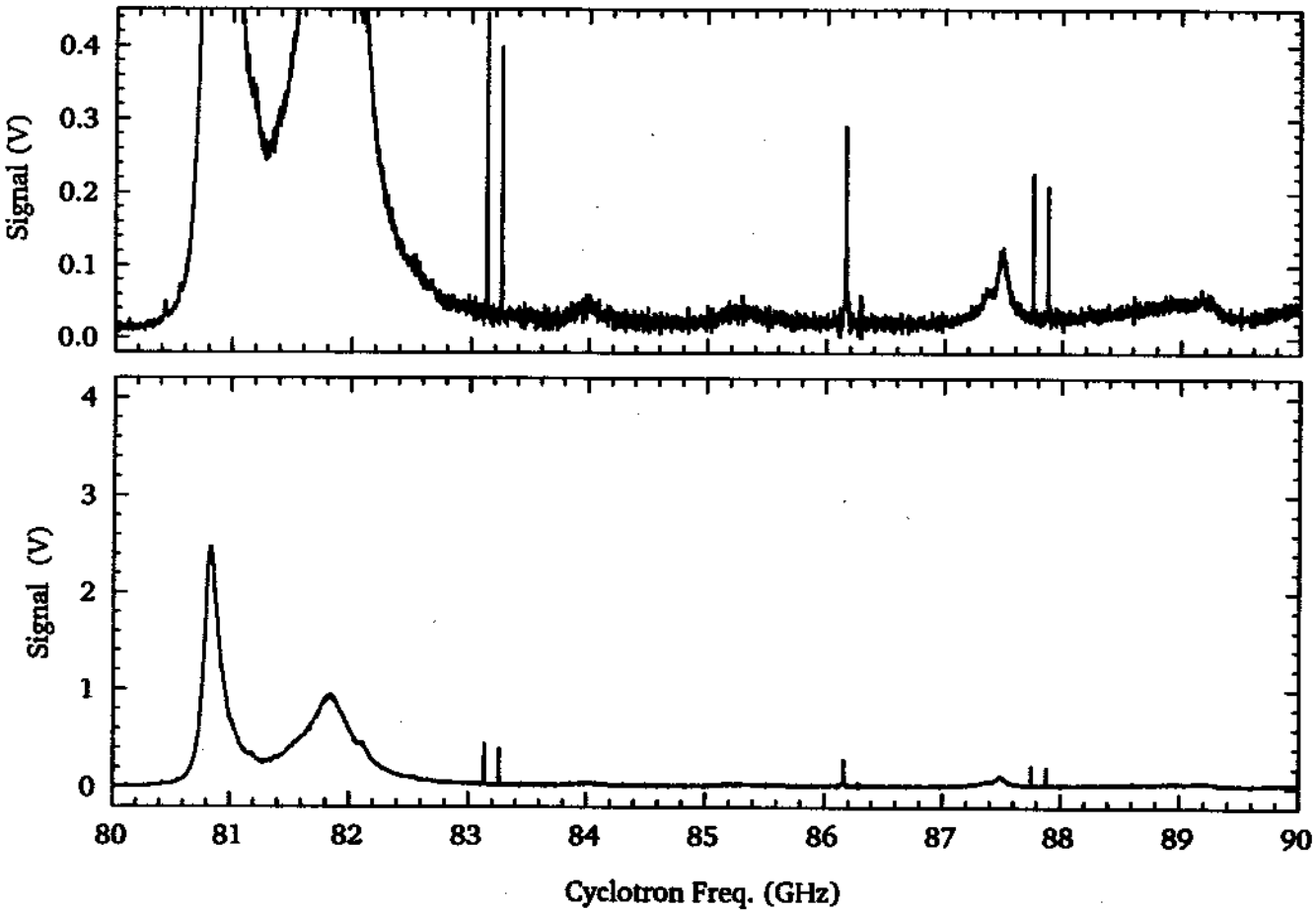
Signal (V)
0.4
0.3
0.2
0.1
0.0
Signal (V)
4
3
2
1
0
80
81
82
83
84
85
86
87
88
89
90
Cyclotron Freq. (GHz)

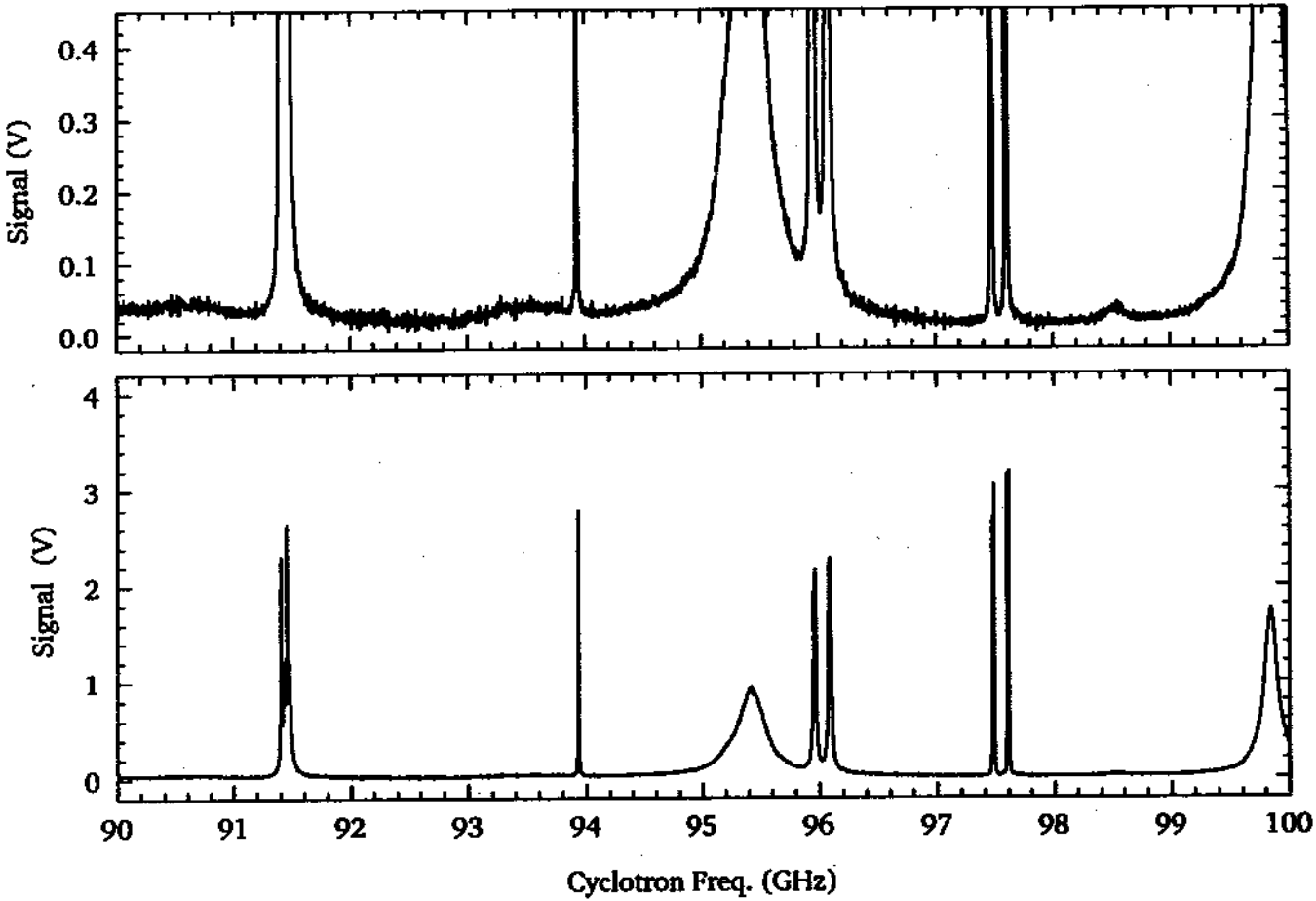
Signal (V)
0.0
0.1
0.2
0.3
0.4
Signal (V)
0
1
2
3
4
90
91
92
93
94
95
96
97
98
99
100
Cyclotron Freq. (GHz)

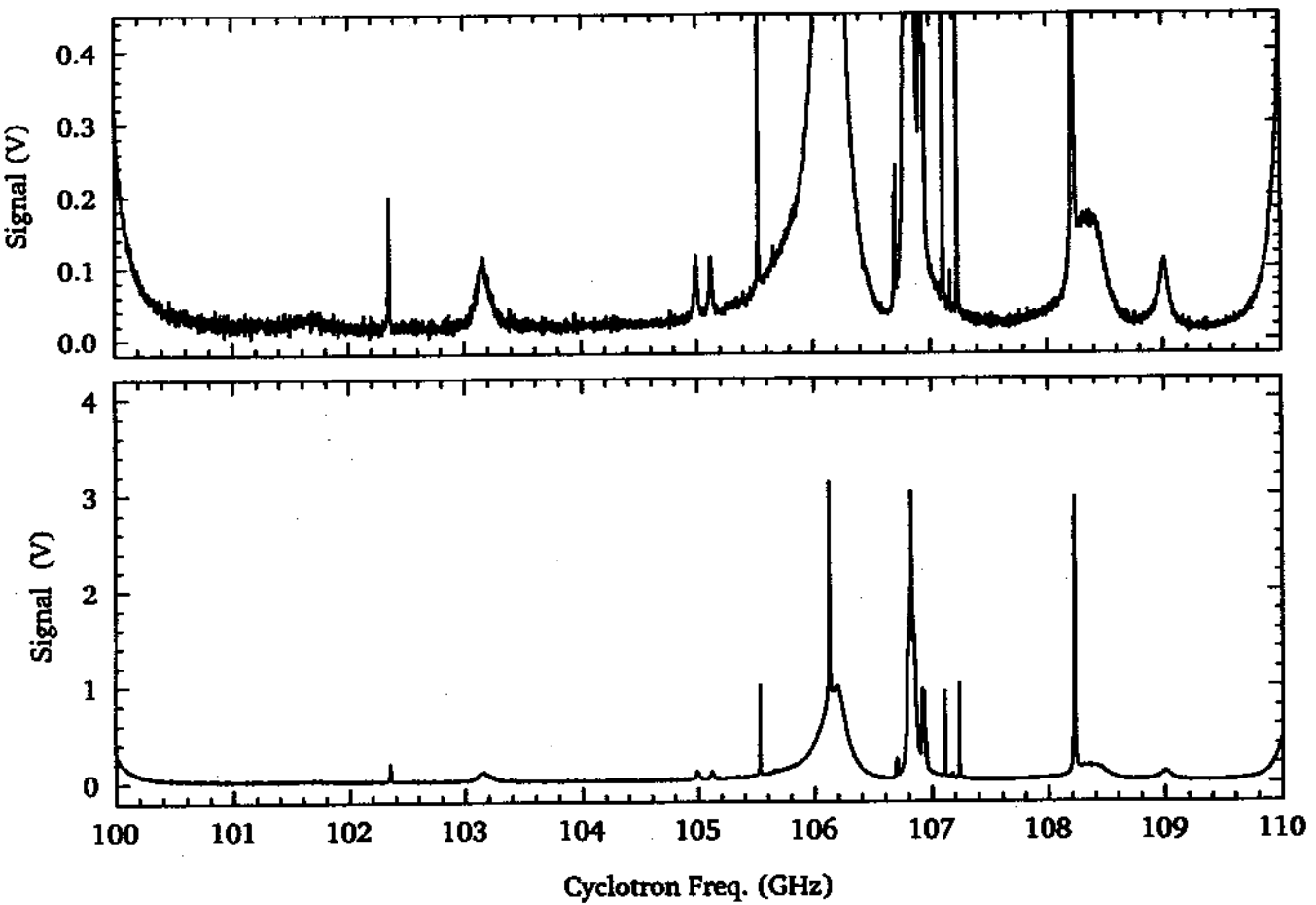
Signal (V)
0.4
0.3
0.2
0.1
0.0
Signal (V)
4
3
2
1
0
100
101
102
103
104
105
106
107
108
109
110
Cyclotron Freq. (GHz)

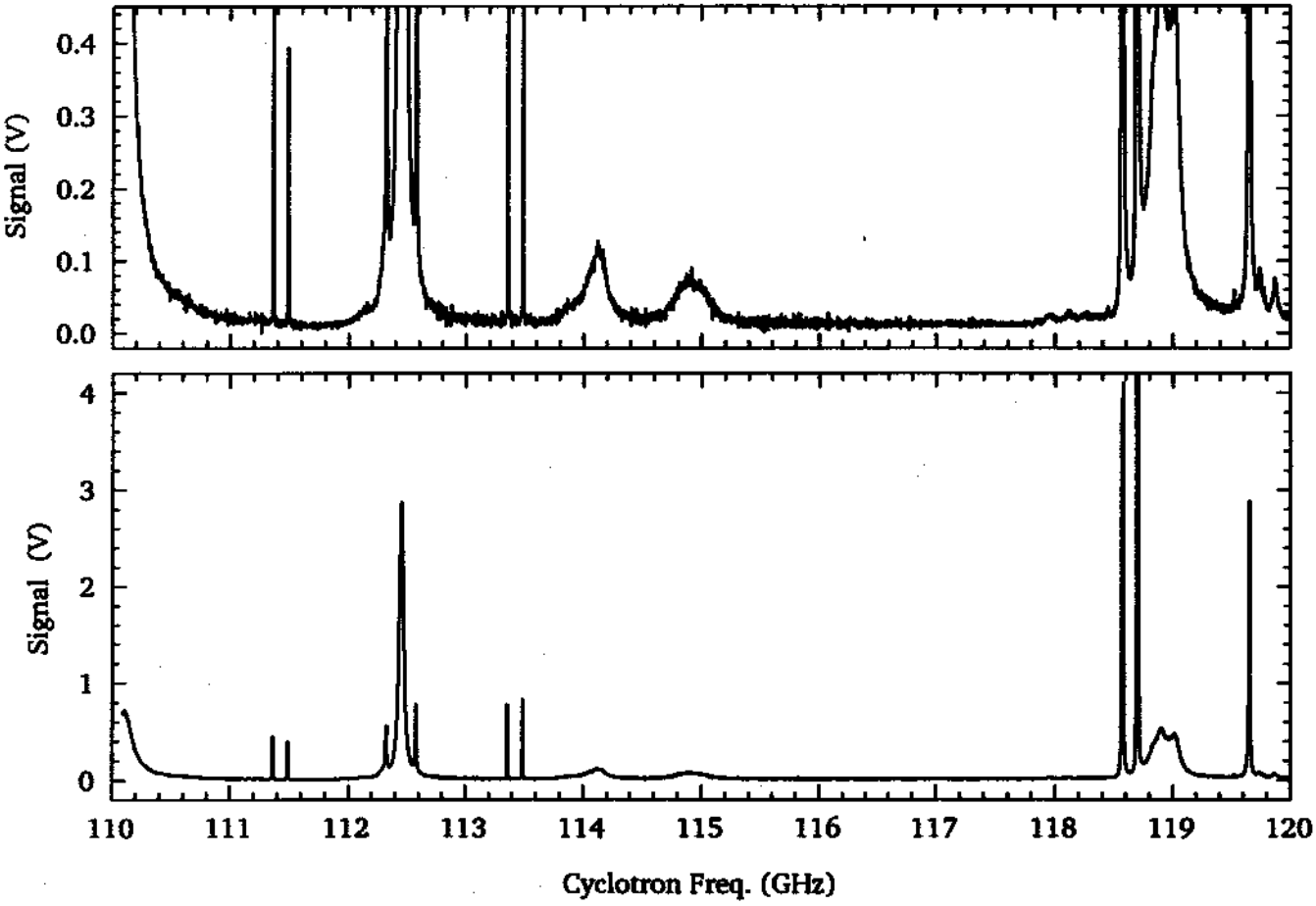
Signal (V)
0.0
0.1
0.2
0.3
0.4
Signal (V)
0
1
2
3
4
110
111
112
113
114
115
116
117
118
119
120
Cyclotron Freq. (GHz)

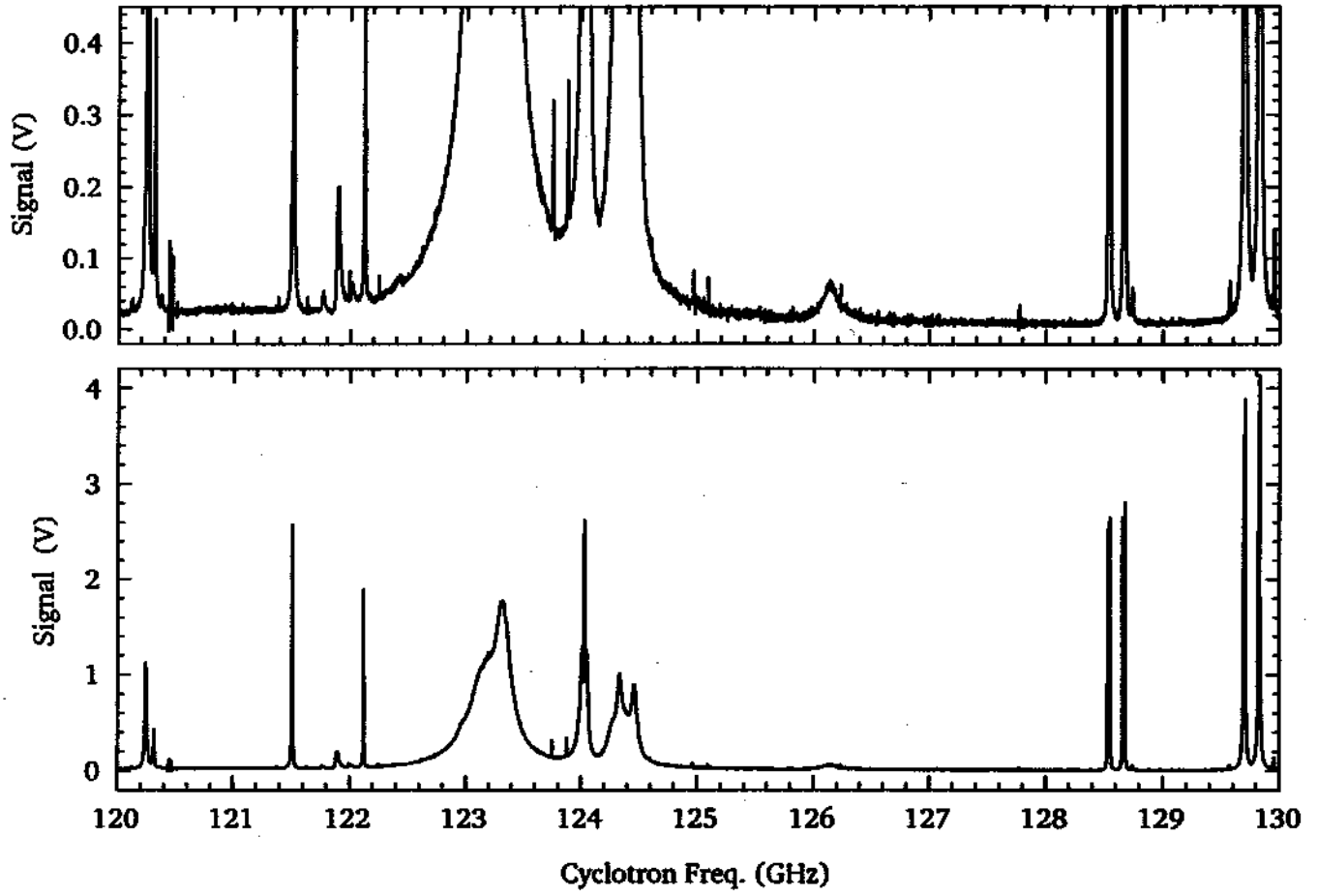
Signal (V)
0.0
0.1
0.2
0.3
0.4
Signal (V)
0
1
2
3
4
120
121
122
123
124
125
126
127
128
129
130
Cyclotron Freq. (GHz)

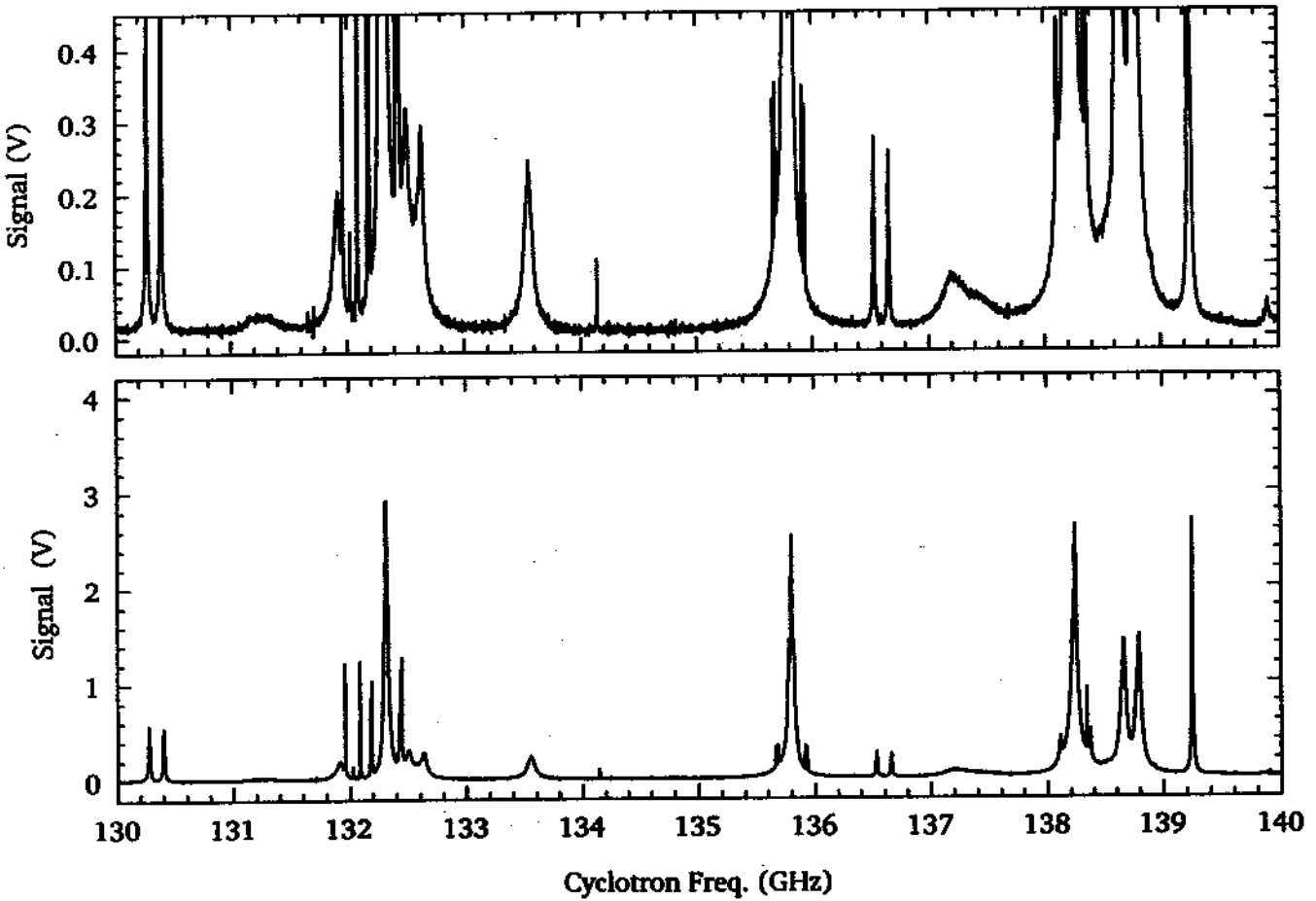
Signal (V)
0.0
0.1
0.2
0.3
0.4
Signal (V)
0
1
2
3
4
130
131
132
133
134
135
136
137
138
139
140
Cyclotron Freq. (GHz)

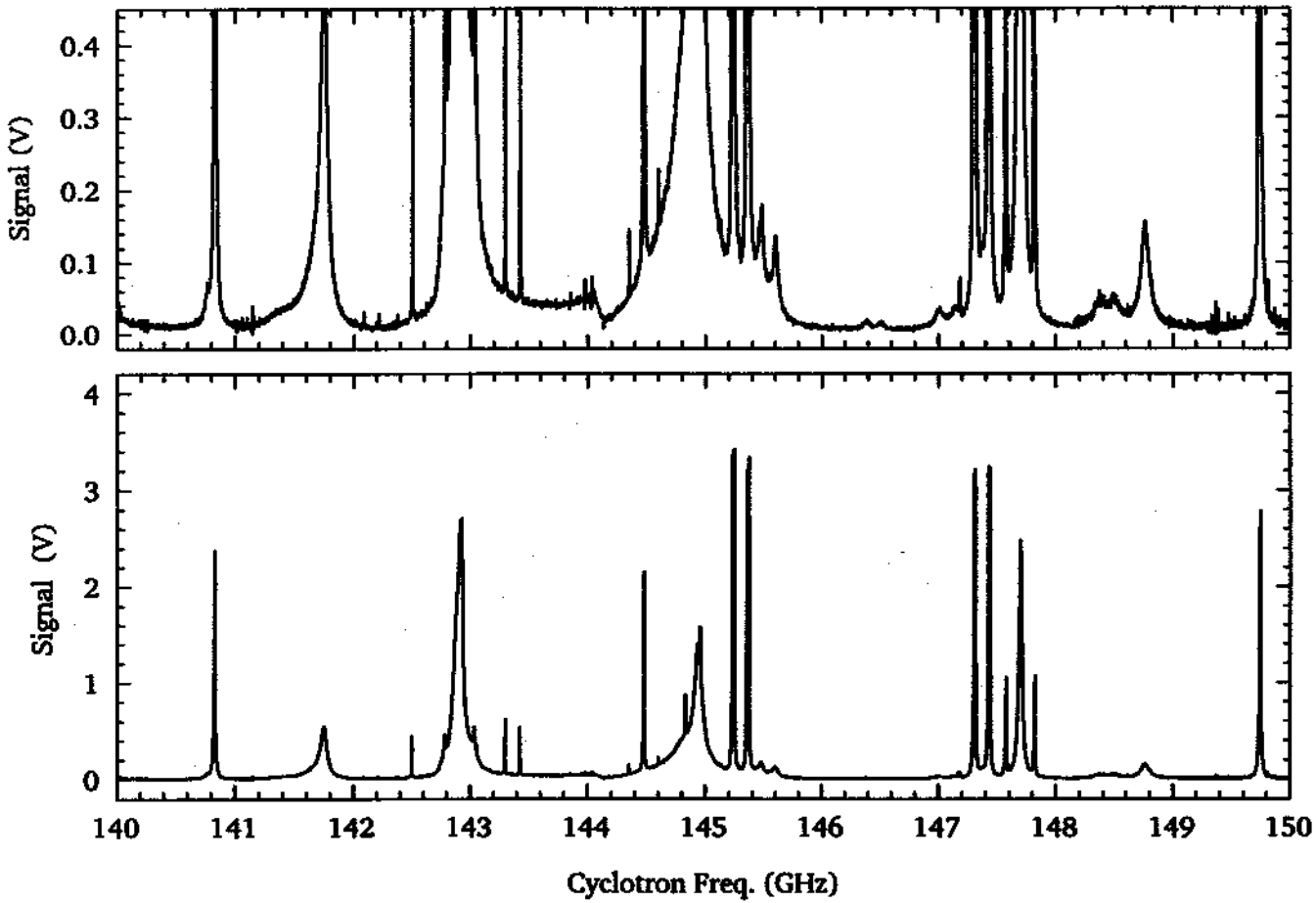
Signal (V)
0.0
0.1
0.2
0.3
0.4
Signal (V)
0
1
2
3
4
140
141
142
143
144
145
146
147
148
149
150
Cyclotron Freq. (GHz)

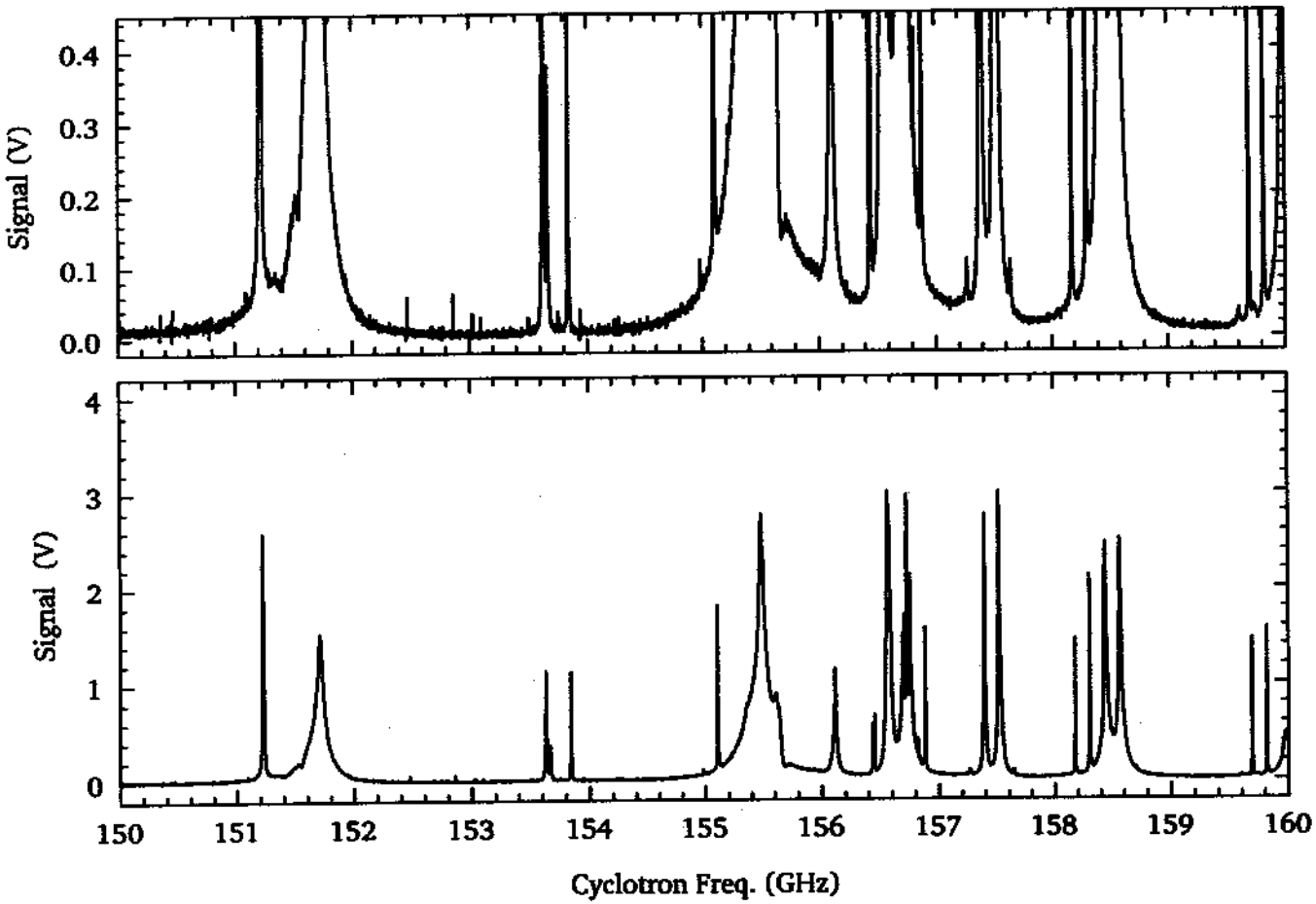
Signal (V)
0.0
0.1
0.2
0.3
0.4
Signal (V)
0
1
2
3
4
150
151
152
153
154
155
156
157
158
159
160
Cyclotron Freq. (GHz)

Signal (V)
0.4
0.3
0.2
0.1
0.0
Signal (V)
4
3
2
1
0
160
161
162
163
164
165
166
Cyclotron Freq. (GHz)

## 4.6 Summary

The observation that spontaneous emission from the cyclotron motion of an electron in a Penning trap cavity [32] is inhibited and subsequent calculations of the corresponding frequency shifts [8,9,11,12] signalled that the most accurate tests of quantum electrodynamics were seriously interrupted by modifications to the QED vacuum. Experiments with synchronized electron oscillators in a new cylindrical trap cavity [78,79] show how to change the cavity-modified vacuum from a serious interruption into an advantage. A new technique for probing electron-cavity interaction employs the sensitivity of the coherent motions of parametrically-pumped oscillators to radiative cooling, allowing the frequencies and quality factors for radiation modes of a trap cavity to be cleanly observed and measured for the first time. Frequencies of more than 100 observed modes below 166 GHz correspond to those of an ideal cavity to typically 1% or better. This makes it possible to identify observed standing wave fields using familiar classifications [49] (e.g. $TE_{115}$). The interaction with standing waves is so well controlled that motional sidebands and splittings are observed due to the axial oscillation of electrons in the electric field gradient of the cavity mode. Modification of resonance lineshape (broadening and splitting) is also observed for strong electron-cavity coupling.

Among identified cavity standing waves are some which couple to an electron's cyclotron motion at the trap center. Others should allow rapid change of cyclotron damping, sideband cooling of an electron to very low (mK) temperatures and directly driven spin flips. The cavity-modified vacuum is an advantage insofar as measured linewidths are narrowed when the electron cyclotron oscillator radiates less than in free space. This is arranged by tuning the magnetic field so that the electron cyclotron frequency is not resonant with the resonant frequency of a cavity mode which couples to the electron. Simple theory yields damping rates (eg. Fig. 1.1a) and frequency shifts (eg. Fig. 1.1b) which can be experimentally confirmed and used to avoid attendant frequency shifts, making possible a new generation of measurements of the electron magnetic moment.